JOURNAL OF PETROLOGY | VOLUME 46 | NUMBER 5 | PAGES 973–997 | 2005 | doi:10.1093/petrology/egi007

Mantle Preconditioning by Melt Extraction during Flow: Theory and Petrogenetic Implications

JULIAN A. PEARCE*

SCHOOL OF EARTH, OCEAN AND PLANETARY SCIENCES, CARDIFF UNIVERSITY, CARDIFF CF10 3YE, UK

RECEIVED JANUARY 4, 2004; ACCEPTED DECEMBER 8, 2004
ADVANCE ACCESS PUBLICATION FEBRUARY 4, 2005

Mantle preconditioning may be defined as the extraction of small melt fractions from mantle asthenosphere during its flow to the site of magma generation. Equations may be written for mantle preconditioning, assuming that the mantle comprises enriched 'plums' in a depleted matrix. The equations take into account variations in mass fraction of plums, the relative rate of melting of plums and matrix, the temperature and pressure of melt extraction, the mass fraction of melt extracted, the extent of chemical exchange between plums and matrix, and the efficiency of melt extraction. Monitoring mineralogical changes and variations in partition coefficients along the inferred P–T–t *path of the mantle asthenosphere allows the equations to be correctly applied to the conditions under which melt extraction takes place. Numerical experiments demonstrate the influence of petrogenetic variables on the shape of melt extraction trajectories and provide new criteria for distinguishing between melt extraction and mixing as the cause of regional geochemical gradients. Representative examples of arc–back-arc systems (Scotia), continental break-up (Afar) and plume–ridge interaction (Azores) indicate that the compositions of the mantle sources of mid-ocean ridge basalts and island arc basalts may be determined, at least in part, by the melt extraction histories of their asthenospheric sources.*

KEY WORDS: *geochemical modelling; mantle flow; isotope ratios; trace elements*

INTRODUCTION

The requirement for conservation of mass leads to the development of pressure gradients that drive horizontal asthenospheric flow on a variety of scales. Thus, asthenosphere must flow towards ocean ridges and regions of active lithospheric extension where material is being removed, but flow away from plumes where material is being added. In addition, asthenosphere must flow obliquely away from converging or colliding continents because the lithospheric keels of the continents act as barriers to flow and prevent return flow in the direction of convergence. At subduction zones, asthenosphere should flow into mantle wedges because of the removal of mantle beneath the arc and above the underlying subducting plate (Davies & Stevenson, 1992). This inflow rate will increase if the slab is rolling back or sinking (Dvorkin *et al.*, 1993). The greatest flow rates are probably from adjacent regions of positive and negative pressure, such as from plumes to ridges (plume–ridge interaction), plumes to incipient oceans (volcanic rifted continental margins) or collision zones to marginal basins (mantle extrusion).

The significance of pressure-driven asthenosphere flow for magma genesis has been recognized for some time through identification of geochemical gradients or geochemical discontinuities. Most of the early work (e.g. Schilling, 1969, 1973) and much recent work (e.g. Douglass *et al.*, 1999; Haase, 2002; Thirlwall *et al.*, 2004) focuses upon the geochemical 'spikes' along the mid-ocean ridge system and the concept of mixing between flowing plume mantle and ambient mid-ocean ridge basalt (MORB) mantle. Over the past decade, however, there has been a growing realization that melt extraction during mantle flow could also play a significant role, and perhaps even the dominant role, in generating regional geochemical gradients. In particular, McCulloch & Gamble (1991) and Woodhead *et al.* (1993) proposed that asthenosphere flowing into the mantle wedge above subduction zones loses a small melt fraction in the back-arc region before melting beneath the volcanic arc, and Phipps Morgan *et al.* (1995) argued that asthenosphere

*Telephone: +44-2920-875124. Fax +44-2920-874326. E-mail: PearceJA@cardiff.ac.uk

moving from plume source to near-ridge sink would encounter thinner and thinner lithosphere and so lose melt to off-axis volcanism before the ridge itself was reached. Others, such as Yu *et al.* (1997) presented geochemical models relating the mantle reaching mid-ocean ridges to melt extraction during flow of plume material towards the ridge.

There have been many proposed refinements to the basic model of melt extraction during mantle flow. Phipps-Morgan & Morgan (1999) proposed that the asthenosphere may be supplied by the melt residues from plumes, rather than by a fertile plume mantle, and that it is these that subsequently melt to form MORB. Niu *et al.* (1999) pointed out that the flowing mantle could lose melt to the overlying mantle lithosphere by infiltration of small melt fractions and thus that off-axis volcanism is not a prerequisite for melt extraction. Haase & Devey (1996) and Harpp & White (2001) emphasized that two types of asthenospheric flow could affect magma genesis: shallow, shear-driven flow caused by movement of the overlying lithospheric plate, and deeper pressure-driven flow caused by plume-to-ridge pressure gradients. Pan & Batiza (1998) noted that melt extraction during mantle flow may be accompanied by entrainment of the mantle above and below the asthenospheric conduit. Murton *et al.* (2002) presented a model of polybaric melt extraction during mantle flow.

The likely mechanism of melt extraction from the mantle has been termed 'dynamic melting' by Langmuir *et al.* (1977) to denote fractional melting with a trapped melt fraction. The studies outlined above imply that dynamic melting may take place in two settings: during asthenospheric flow to the principal site of magma generation, and at the principal site of melt generation itself (in the melting column). The mantle itself need not 'see' this distinction as it loses its incompatible elements in a broadly similar way during both processes. However, for the extracted magma, there is an important difference as only the melt fractions extracted within the melting column have the opportunity to contribute to the pooled melt produced at the site of magma generation.

Kincaid & Hall (2003) usefully distinguished between these two settings of melt extraction by describing melt extraction during flow to the site of magma generation as 'preconditioning', the terminology adopted for this paper. Kincaid & Hall (2003) specifically investigated arc–basin systems, in which mantle may be preconditioned by loss of melt fractions in the back-arc before undergoing melting beneath the arc front. However, mantle may be preconditioned in any setting if its temperature exceeds its solidus during flow to the eventual site of magma genesis—as illustrated in Fig. 1. Thus it is possible that the mantle source region for any asthenosphere-derived magma will reflect not just the provenance of its source, or mixture of sources, but also its history of preconditioning by melt extraction.

This paper examines the potential relationships between asthenosphere flow and mantle composition, with particular emphasis on the geochemistry and petrology of preconditioning and the implications of preconditioning for magma genesis in a range of tectonic settings.

MANTLE PRECONDITIONING BY MELT EXTRACTION: THEORY

The fundamental assumption in modelling mantle preconditioning is that the mantle comprises a mixture of enriched and depleted components (e.g. Sleep, 1984; Zindler *et al.*, 1984; Allègre & Turcotte, 1986). Much of this work treats the mantle as a two-component system, made up of enriched 'plums' embedded within a depleted matrix (Phipps Morgan, 1999), although it will also demonstrate that the same approach applies to multi-component systems. It is the preferential removal of these plums during melt extraction that provides the distinctive geochemical features of mantle preconditioning.

Phipps Morgan (1999) first laid out the basic principles for discriminating between mixing and melt extraction for explaining geochemical gradients between plume and depleted MORB mantle. He defined 'melt extraction trajectories', or 'METs', as trajectories in element-isotope space resulting from progressive extraction of melt from a heterogeneous source. He demonstrated that they could have the superficial appearance of mixing trajectories, but found that melt extraction and mixing could be distinguished in 'two component, two element + isotope systems'. This paper takes his approach as the starting point, retaining also his symbols (T_i and I_i for trace element concentration and isotope ratio for element i and $T_{i/j}$ for the trace element ratio i/j) and extends it to permit the use of numerical experiments to study the effect of varying the different melt extraction parameters.

The first stage of the preconditioning model is to define the starting composition of the mantle asthenosphere (A) as a two-component mixture of 'plums' (P) and matrix (M) containing a mass fraction M_P of plums, and hence a mass fraction $(1 - M_P)$ of matrix. Making a small approximation by ignoring the fact that the element in the isotope ratio has two different masses, the trace element ratio, $T_{2/1}$, and isotope ratio, I_1, of the asthenosphere can be expressed as mixing equations, corresponding to equation (1) of Phipps Morgan (1999):

$$T^{A}_{2/1} = \frac{T^{P}_{2} M_P + T^{M}_{2}(1 - M_P)}{T^{P}_{1} M_P + T^{M}_{1}(1 - M_P)} \quad (1)$$

$$I^{A}_{1} = \frac{T^{P}_{1} M_P I^{P}_{1} + T^{M}_{1}(1 - M_P) I^{M}_{1}}{T^{P}_{1} M_P + T^{M}_{1}(1 - M_P)}. \quad (2)$$

Phipps Morgan (1999) modelled his melt extraction trajectories by allowing the two components to change

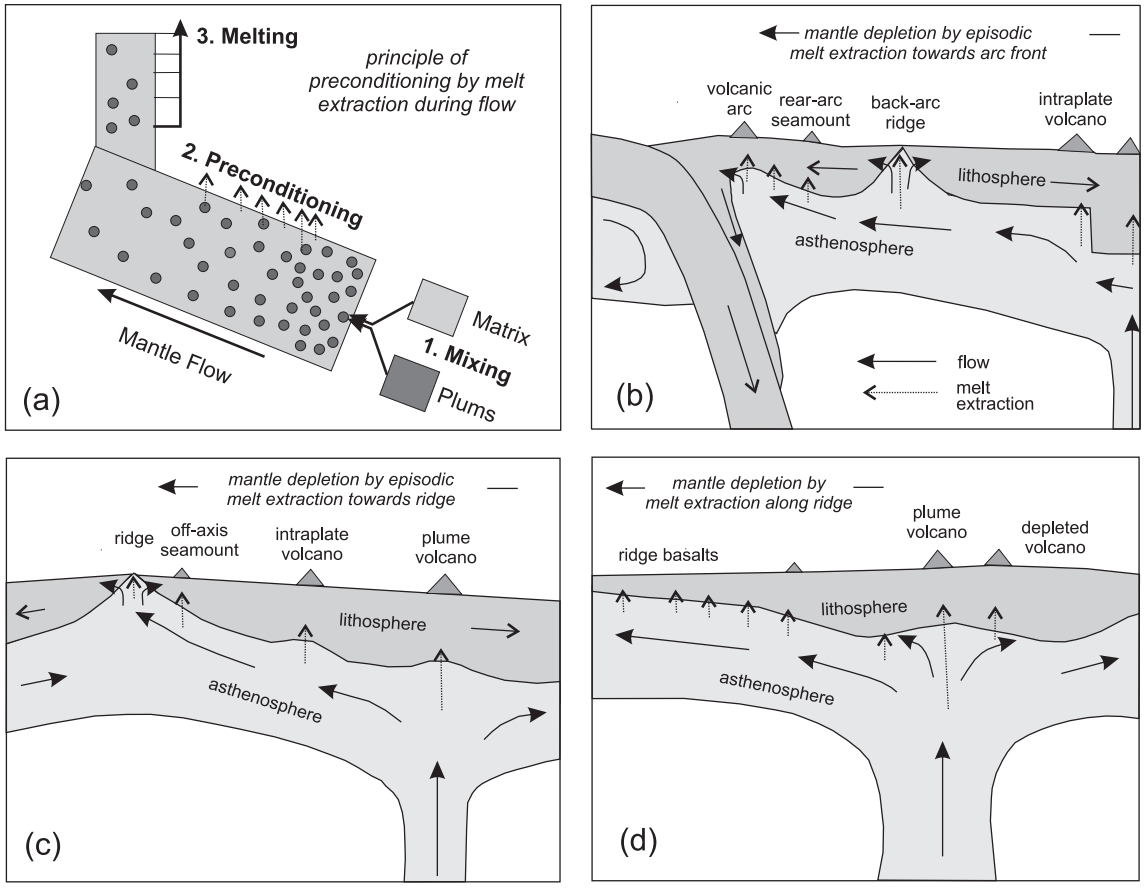

Fig. 1. Illustration of the concept of mantle preconditioning. In (a), heterogeneous asthenosphere, created by mixing of matrix and plums in an unspecified part of the mantle, undergoes preconditioning by loss of small melt fractions by decompression during flow to the site of magma genesis. Typically, the effect of preconditioning is to reduce the contribution of the plums as they usually have the lower solidi. (b)–(d) show three examples of areas where mantle may be preconditioned before reaching its ultimate site of magma generation. In (b) [the original preconditioning concept of McCulloch & Gamble (1991)], mantle is preconditioned during decompression at the point of entry into the arc–basin system, and in the back-arc and rear arc, before reaching the melting column at the arc front. In (c) [concept of Pan & Batiza (1998)], mantle flowing from a plume to a ridge is preconditioned during initial plume upwelling, and subsequently during off-axis decompression, before entering the axial melting column. In (d) [concept of Murton *et al.* (2002)], mantle flowing from a plume along a ridge is preconditioned during initial plume upwelling, and then continuously during along-ridge flow. In all cases, the lavas sourced by progressively preconditioned mantle along the mantle flow lines give melt extraction trajectories (Phipps Morgan, 1999) in geochemical space. Thus preconditioning provides an alternative explanation to mixing as a cause of regional geochemical gradients.

their compositions by undergoing sequential increments of dynamic melting. His key assumptions are that plums melt independently of the matrix component (as they must do in part, at least if melt extraction trajectories are to have isotope gradients) and that the plum and matrix components each lose a different mass fraction of melt.

This work extends his formulation. It first defines the mass fraction of melt lost from the plum component relative to the mass of the plum component as F_P and the mass fraction of melt lost from the matrix component relative to the mass of the matrix component as F_M. This means that, after extraction of a total melt fraction F_L from a mass fraction M_P of plums plus a mass fraction $(1 - M_P)$ of matrix, the total mass will be $1 - F_L$ made up of a mass fraction $1 - F_P$ of plums and $1 - F_M$ of matrix. The mass fractions of plums and matrix remaining will then be given by $\frac{M_P(1-F_P)}{(1-F_L)}$ and $\frac{(1-M_P)(1-F_M)}{(1-F_L)}$, respectively.

The basic equations for trace element ratios ($T_{2/1}$) and isotope ratios (I_1) in preconditioned mantle asthenosphere following a given episode of melt extraction can thus be expressed, again using mass balance, as

$$T_{2/1}^{A^*} = \frac{T_2^{P^*} M_P(1-F_P) + T_2^{M^*}(1-M_P)(1-F_M)}{T_1^{P^*} M_P(1-F_P) + T_1^{M^*}(1-M_P)(1-F_M)} \quad (3)$$

$$I_1^{A^*} = \frac{T_1^{P^*} M_P(1-F_P) I_1^P + T_1^{M^*}(1-M_P)(1-F_M) I_1^M}{T_1^{P^*} M_P(1-F_P) + T_1^{M^*}(1-M_P)(1-F_M)} \quad (4)$$

where A* refers to ratios in the composite residual mantle asthenosphere after an episode of melt extraction, P* to concentrations in the residual 'plum' end-member and M* to concentrations in the residual matrix end-member. The trace element concentrations (T_1 and T_2) in the residues can be modelled using Shaw's (1970) fractional melting equation, and porosity can be taken into account by calculating bulk distribution coefficients that include trapped melt with $D = 1$ (see Appendix A for details).

Because the plums and matrix probably melt at different rates, it is useful to define a relative rate of melting, r, such that $r = F_M/F_P$. Thus, $r = 0$ if only the plums are melting and $r = 1$ if plums and matrix melt at the same rate. Also, r may approximate to a constant during preconditioning because the amount of melt extracted is low, although it may vary considerably once the solidus for the pure matrix is exceeded at the higher degrees of melt extraction found within a melting column (Phipps Morgan, 2001). F_P and F_M can be expressed in terms of M_P (the mass fraction of plums in the starting material), F_L (the total mass fraction of melt extracted from the asthenosphere during flow) and r (the relative contribution of plum melt to total melt). By mass balance

$$F_L = M_P F_P + (1 - M_P) r F_P$$

$$\text{so } F_P = z F_L$$

$$\text{where } z = 1/(M_P + r - r M_P).$$

Substitution for F_P and F_M into equations (3) and (4) gives general equations for mantle preconditioning by melt extraction during flow in which F_L, r and M_P are the principal variables:

$$T_{2/1}^{A^*} = \frac{T_2^{P^*} M_P (1 - z F_L) + T_2^{M^*} (1 - M_P)(1 - r z F_L)}{T_1^{P^*} M_P (1 - z F_L) + T_1^{M^*} (1 - M_P)(1 - r z F_L)} \quad (5)$$

$$I_1^{A^*} = \frac{T_1^{P^*} M_P (1 - z F_L) I_1^P + T_1^{M^*} (1 - M_P)(1 - r z F_L) I_1^M}{T_1^{P^*} M_P (1 - z F_L) + T_1^{M^*} (1 - M_P)(1 - r z F_L)}. \quad (6)$$

Figure 2 illustrates the geochemical principles of mantle preconditioning using equations (5) and (6) by examining some hypothetical melt extraction trajectories on plots of isotope ratio against trace element ratio. Two projections are shown: (a) isotope ratio, I_1, against trace element ratio, T_2/T_1, in which T_1 is more incompatible than T_2 (e.g. $^{143}Nd/^{144}Nd$ against Yb/Nd or Sm/Nd, or $^{176}Hf/^{177}Hf$ against Lu/Hf); (b) isotope ratio, I_1, against trace element ratio, T_2/T_1, in which T_1 is less incompatible than T_2 (e.g. $^{143}Nd/^{144}Nd$ against La/Nd or $^{176}Hf/^{177}Hf$ against Nb/Hf).

In Fig. 2a, the initial composition lies at a_o on a mixing trend between plums and matrix. Because of the common denominators in the ratios used in the two axes, this mixing trend will be linear (Langmuir *et al.*, 1977). Both plums and matrix will then become relatively depleted in the more incompatible trace element with progressive melt extraction. As T_1 is more incompatible than T_2, the T_2/T_1 ratios of both matrix and plums will increase

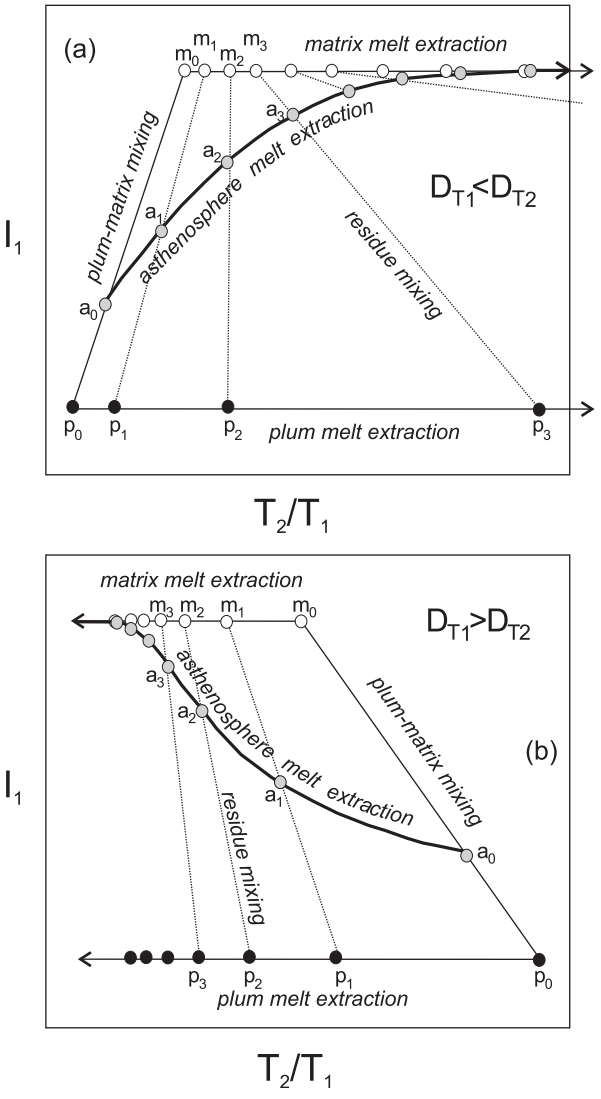

Fig. 2. Principles of modelling preconditioning by melt extraction from two-component (plum + matrix) mantle in isotope–trace element ratio space. In (a), the trace element T_1 is less incompatible than T_2 whereas, in (b) it is less incompatible. In both cases, the plum component is melted out more rapidly than matrix. If m_0–p_0 represents the mixing between matrix and plums in the mantle before preconditioning, then the matrix residues will follow trajectory m_0–m_3 while the plum residues follow trajectory p_0–p_3. The preconditioned asthenosphere will then follow the trajectory a_0–a_3, at a shallower angle than the original plum–matrix mixing line. Its topology reflects a decreasing plum influence with increasing melt extraction. Eventually it will reach a plateau where the plum residues (while still present) contain so little T_1 that the isotope ratio is entirely determined by the matrix ratio.

and, because the plums melt the more rapidly, the $\mathcal{T}_2/\mathcal{T}_1$ ratios of the plums will increase more rapidly than those of the matrix. The isotope ratio will move towards the ratio of the component that melts out less rapidly; that is, towards the ratio of the matrix in this case. The bulk asthenosphere composition must then lie on tie-lines joining the residual matrix and residual plum compositions. Thus, in this model, the residual asthenosphere composition will lie at a_1 on tie-line m_1–p_1 after extraction of the first mass fraction of melt, at a_2 on tie-line m_2–p_2 after extraction of a second mass fraction, and so on. The melt extraction trajectory is the line a_0–a_3.

Eventually, the plums will either melt out or become so depleted that they make no effective contribution to the bulk composition. The melt extraction trajectory will then flatten at the isotope ratio of the matrix (as shown in Fig. 2a)—unless there has been isotopic exchange between plums and matrix, in which case it will flatten at an isotope ratio between that of the matrix and that of the plums as discussed later.

On the second isotope–trace element projection (Fig. 2b), the ratio $\mathcal{T}_2/\mathcal{T}_1$ decreases with progressive melt extraction as $\mathcal{T}_1$ is now less incompatible than $\mathcal{T}_2$. The resulting melt extraction trajectory is concave rather than convex and converges on a trace element ratio of zero rather than diverges towards infinity.

The essential characteristic of preconditioned 'plum-pudding' mantle in which plums undergo preferential melting is therefore a convergence on the isotopic composition of the matrix coupled with trace element ratios that converge to zero or infinity depending on which element is the more incompatible. This simple model does, however, assume a single plum composition while ignoring entrainment of other mantle compositions, equilibration between the plum and matrix components and efficiency of melt extraction. The next sub-sections consider the effects of these complexities.

Preconditioning of multi-component mantle

Although this paper focuses on the simple case of a two-component (melt + matrix) mantle, the method can be extended to multi-component mantle. Mathematically, the various single plume contributions to the trace element and isotope budgets in equations (5) and (6) must be modified by substituting multiple plum contributions. For example, for a residual asthenosphere containing a number of plum components, P_i^*, with $F_{P_i}/F_L = z_i$, the term $\mathcal{T}_2^{P^*} M_P(1 - zF_L)$ in equation (5) must be replaced by $\sum[\mathcal{T}_2^{P_i^*} M_{P_i}(1 - z_i F_L)]$.

Figure 3a illustrates the effect of adding a second plum component to the melt extraction equations for the case of I_1 against $\mathcal{T}_{2/1}$ where $\mathcal{T}_1$ is more incompatible than $\mathcal{T}_2$ (as in Fig. 2a). In this example, the second plum, Q, melts twice as fast as P, although both melt faster than the matrix. The bulk plum composition evolves along trajectory p_0–p_3, converging isotopically upon the type of plum that melts less rapidly, namely P. The composition of the residual asthenosphere must then lie on tie-lines between the residual matrix composition and the residual bulk plum composition at the points determined by two-component (residual bulk plum–residual matrix) mixing. The resulting melt extraction trajectory, a_0–a_3, will then be the locus of residual asthenosphere compositions. In this case, the plums are more similar in composition to each other than to the matrix, so the trajectory for multi-component mantle resembles that of two-component mantle. Phipps Morgan (1999) reached the same conclusion from examining the isotopic consequences of melting mantle containing a range of plum components (e.g. HIMU, EMI, EMII) melting at different rates. He found that melt extraction from a multi-component system can produce a tube-like MET in isotope space. He also noted that melt extraction may provide a better explanation than multi-component mixing for ocean island isotope systematics.

Preconditioning with entrainment

Flowing asthenosphere may entrain overlying lithosphere or underlying mesosphere in addition to undergoing melt extraction. If so, then the models require modification. Entrainment at any point on the melt extraction trajectory simply moves the asthenosphere along a linear mixing trend towards the entrained composition. It can be modelled by iterating mixing and melt extraction equations.

Figure 3b illustrates combined preconditioning and entrainment, again for the case of I_1 against $\mathcal{T}_{2/1}$ where $\mathcal{T}_1$ is more incompatible than $\mathcal{T}_2$. The gradient will be affected in different ways according to the precise composition of the mixing component. For example, entrainment of matrix will shift the melt extraction trajectory towards the matrix composition. Conversely, entrainment of the starting asthenosphere composition will usually shift the trajectory towards the plum composition. This latter process is likely to be important if preconditioned asthenosphere has the opportunity to mix with deeper asthenosphere that has not risen above its solidus and so had no history of preconditioning.

Preconditioning with chemical exchange between plums and matrix

A recent study by Kogiso *et al.* (2004) concluded that partial melts segregate from the mantle without significant diffusive equilibration between the melt and their peridotite residues. However, although it is possible that the plums and matrix behave as completely independent

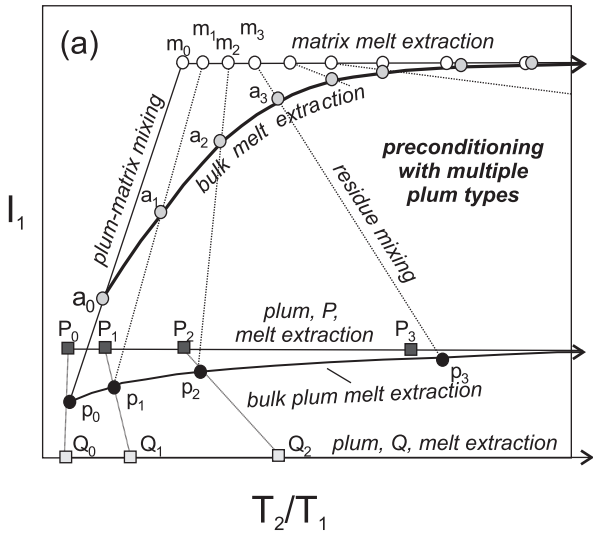

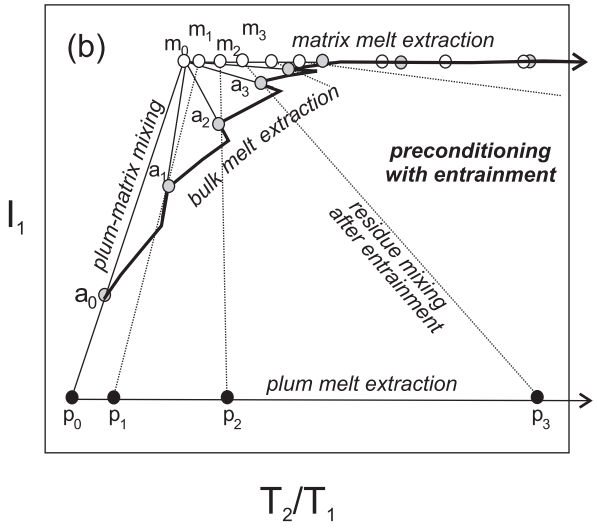

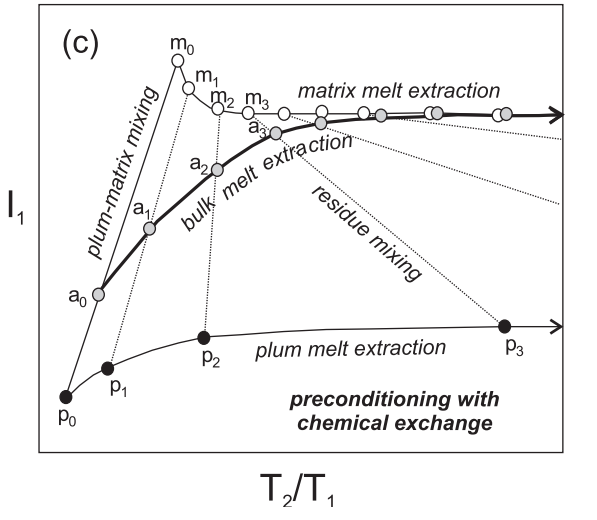

and isolated units during preconditioning and melting, it is still important to evaluate the possibility that some form of chemical exchange takes place. Given the evidence that diffusion is too slow, this work focuses on mass transfer to effect chemical exchange between plums and matrix.

The approach adopted here is to assume that, during each episode of melt extraction, a small mass fraction of the pooled melt is retained by both plums and matrix. This pooled melt will have isotope ratios and element concentrations between those of the two end-members and so allow isotope and element redistribution between plums and matrix: the matrix will be enriched in incompatible elements while the plums are depleted. Of course, chemical exchange will really be more complicated than this. For example, in a flowing, decompressing system, the upper part of the asthenosphere might be expected to be invaded by melts from deeper in the asthenosphere (e.g. Murton *et al.*, 2002). However, the method proposed (addition of trapped melt after melt extraction) provides a convenient way to model variable chemical exchange between matrix and plums. It requires that the extraction equations be modified by adding a trapped melt component to the trace element and isotope budgets in equations (5) and (6), as described in Appendix A.

Figure 3c illustrates the effect of including chemical exchange in the melt extraction models. Essentially the 'plums' converge isotopically on the matrix composition during flow, while the matrix converges on the plum composition. The change in the slope of the melt extraction trajectory is small, but there is a significant change in the isotope composition reached when plums have effectively been removed. Thus, if $r < 1$, the greater the proportion of trapped melt, the lower the final isotope ratio of the preconditioned mantle.

Preconditioning and efficiency of melt extraction

Efficiency of melt extraction is an important variable in the application of the melt extraction equations. It can be modelled simply as the mass fraction of melt (ϕ) that

Fig. 3. Variations on the principles of modelling of melt extraction. (a) examines the effect of increasing the number of plum components from one to two (P and Q). In this case, melt is extracted more rapidly from Q than from P. Thus the bulk plum residues follow the trajectory p_0–p_3, and the preconditioned asthenosphere follows the trajectory a_0–a_3. (b) incorporates mantle entrainment so that the asthenosphere changes composition by combined mixing and preconditioning. In this illustration, mixing is episodic and of a matrix composition. The net effect is to displace the preconditioning trajectory of the asthenosphere towards the composition of the mantle being mixed. (c) incorporates chemical exchange between matrix and plums. The result is that the trajectory for melt extraction from the matrix converges on the plum isotope composition and vice versa. The principal effect is that the plateau, which forms when only the matrix contributes to the preconditioned asthenosphere, is displaced towards the isotope composition of the plums.

accumulates prior to melt extraction. This appears in the equation for the bulk distribution coefficient (see Appendix A). When the mantle releases melt immediately upon reaching the solidus (efficient melt extraction), ϕ is small and the bulk distribution coefficient for the most incompatible elements is little affected. However, if significant melt accumulates before extraction so that ϕ is large (inefficient melt extraction), then the bulk distribution coefficient for the most incompatible elements will be significantly increased. In Fig. 3, a large value of ϕ would mean that the more highly incompatible element, T_1, is retained to a greater extent by the mantle residue. The T_2/T_1 ratio (where $D_{T_2} > D_{T_1}$) is therefore depleted less rapidly. The net effect is that the melt extraction trajectory is displaced to the left and steepened.

Melting of preconditioned mantle

Mantle that has undergone preconditioning during flow will eventually reach the site of melting (the melting column) to produce the observed, erupted lavas (Fig. 1a). As noted in the Introduction, dynamic melting of heterogeneous mantle may take place both during preconditioning and within the melting column. The melting column processes may thus, to a first approximation, be modelled in the same way as preconditioning using equations (5) and (6). The mantle composition will, therefore, continue to follow a preconditioning trajectory as it releases melt fractions to the pool of segregating melt in the melting column. It may not, however, be a perfect extrapolation of the preconditioning trajectory as the relative rates of melting of matrix and plums, r, may change markedly as melting proceeds (Phipps Morgan, 2001). In addition, the different plum components may vary in importance as melting proceeds, giving discontinuities on isotope–isotope plots and, to a lesser extent, on isotope–trace element ratio plots (Phipps Morgan, 1999).

The relationship between the primitive magma emerging from the melting column and the composition of the mantle entering the column will then depend on (1) initial mantle heterogeneities caused by variable mixtures of the components, (2) the extent of, and variability in, preconditioning, and (3) the extent of pooling of the various melt fractions. Figure 4 illustrates the principles underlying the dynamic melting of preconditioned mantle. It again focuses on the projection of isotope ratio (I_1) against trace element ratio (T_2/T_1), where element T_1 is less incompatible than T_2 (see Fig. 2a), although the principles apply to all projections.

Figure 4a illustrates the melting of uniformly preconditioned mantle, in which the initial asthenosphere at a_0 has lost melt fractions to reach a_3 prior to reaching the melting column; a_3 then lies on the tie-line between depleted matrix at m_3 and depleted plums at p_3. The melting

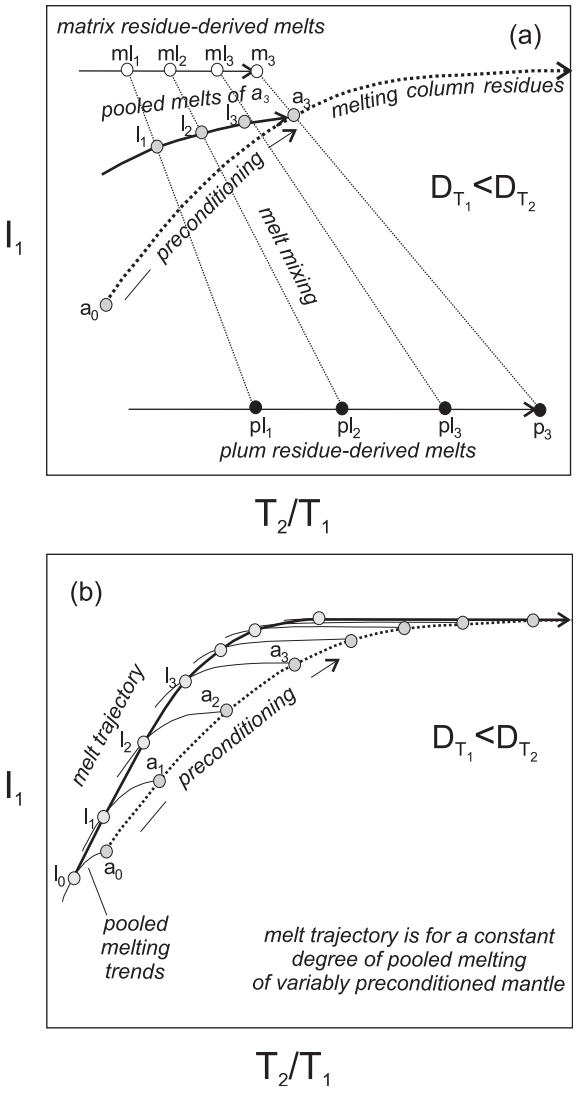

Fig. 4. Principles of modelling of partial melting of two-component mantle. (a) shows the trend of pooled melts (l_3–l_1) extracted from preconditioned mantle (a_3) of a constant composition by varying degrees of melting. Each pooled melt can be viewed as a mixture of matrix-derived and plum-derived melts. Because the plums melt more rapidly, the isotope ratio of the pooled melt is closer to that of the plums at low degrees of melting, but the overall trend is shallower than the preconditioning trajectory. (b) shows the trend of pooled melts extracted from variably preconditioned mantle (a_0–a_3) at a constant degree of melting. The trend is steeper than the preconditioning trajectory until the plateau is reached.

process can be viewed as melting of m_3 and p_3 followed by mixing of the melt fractions generated by each in proportions defined by r, the relative rates of melting of matrix and plums, and M_P, the mass fractions of plums. Mass balance dictates that the overall mass fraction of melt, F, is made up of $F(1 - M_P)r/[r + (1 - r)M_P]$ of matrix-derived melt and $FM_P/[r + (1 - r)M_P]$ of plum-derived melt. Thus, in Fig. 4a, the plum melt

contribution follows the trend pl_1–pl_3–p_3 and the matrix melt contribution follows the trend ml_1–ml_3–m_3, while the pooled melt follows a trajectory l_1–l_3–a_3. At any given degree of melting, the pooled melt, l_i, will lie on a tie-line joining the plum and matrix melts, pl_i and ml_i. If, as is likely, $r < 1$, the early melts will have more plum-like isotope ratios and the pooled melt trajectory will be convex. Appendix A gives the expression for calculating these pooled melt compositions.

Figure 4b extends this principle to the melting of variably preconditioned mantle, in which four parts of an initial mantle asthenosphere at a_0 have lost melt fractions to reach a_1, a_2, a_3 and a_4 so that the melting column is fed by a mantle source with preconditioning-induced heterogeneities. If each mantle composition then undergoes pooled fractional melting, the melt extracted from each will form a series of trajectories, each similar to that in Fig. 4a. If the degree of melting is similar in each case, a trajectory can be drawn to link the compositions of the extracted melt, l_1–l_4. For $D_{T_1} < D_{T_2}$, as here, the overall pooled melt trajectory will lie to the left of, and be steeper than, the melt extraction trajectory. If $D_{T_2} < D_{T_1}$, the equivalent trajectory will lie to the right of the melt extraction trajectory.

It should be noted that trajectories such as that in Fig. 4b also apply to dynamic melting within the melting column when melt fractions are imperfectly pooled. However, the variations in isotope and trace element ratios in lavas produced by mantle dynamic melting of two-component mantle should still be much less than those achieved by preconditioning in most cases—although there may be exceptions as Elliott *et al.* (1991) demonstrated for Iceland. This is because the individual melt increments are always pooled to some extent. However, the net effect is that both preconditioning and dynamic melting may contribute to observed melt extraction trajectories.

MANTLE PRECONDITIONING BY MELT EXTRACTION: MELTING PARAMETERS

In flowing from its original site of matrix–plum mixing to its eventual site of melting and magma generation, the asthenosphere will follow a *P*–*T*–*t* path. If this path intersects its solidus, then melt will be generated and may satisfy physical criteria for extraction. This may be a single event, but could take place over a wide pressure interval, and could involve more than one episode of extraction or continuous extraction. This means that the mineralogical and chemical compositions of the asthenosphere must be tracked along the *P*–*T*–*t* path so that the correct bulk distribution coefficients are used in the modelling. To track these changes simply, this work uses experimental mineral compositions plotted in CaO–Al_2O_3 space. Given that the mantle components may behave differently from plums, it tracks separately the peridotite matrix and two types of plum: pyroxenite/eclogite and hybrid mantle. Having established the mineral composition, it is then possible to calculate partition coefficients and mineral reaction coefficients appropriate for the pressures, temperatures and compositions along the melt extraction (preconditioning) path. For reasons of space this paper focuses on the elements Nd (T_1) and Yb (T_2), but the principles can be applied to any elements.

Tracking matrix mantle mineralogy

Figure 5a illustrates the method used here to model matrix mantle. It is difficult to identify actual samples of matrix mantle as all mantle may contain, or have contained, a plum component. None the less, a good starting point will be mantle that will act as a source for depleted magma such as normal (N)-MORB, either a synthetic material such a MORB pyrolite or a natural occurrence of an unmelted and unenriched peridotite. The majority of potential matrix compositions fall in the range of CaO = 3·5 ± 0·25 and Al_2O_3 = 4·25 ± 0·25. This range also encompasses many of the experimental peridotite compositions used to investigate the anhydrous peridotite solidus. The mean is very similar to Tinaquillo peridotite with its inferred 7% melt loss 'restored', and to the Kettle River Peridotite used in the experiments of Walter (1998). This paper therefore uses CaO = 3·5 and Al_2O_3 = 4·25 (point M in Fig. 5a) for modelling and uses published experiments on mantle similar to this composition to define the compositions of the host minerals at the various pressures and temperatures.

The mineral proportions for any point on a *P*–*T*–*t* path along the solidus of M may be represented graphically in CaO–Al_2O_3 space by the location of M within the polygon formed by the component phases. If (as for 4–6 GPa in Fig. 5a) there are three phases, the proportions may be determined uniquely as there are two variables (CaO and Al_2O_3) and two degrees of freedom (three mass fractions summing to unity). If there are four phases (as for 1–3 GPa in Fig. 3a) the mass fraction of one of these must be determined independently before the proportions of the remainder can be computed from CaO and Al_2O_3 concentrations.

Figure 5a shows that only olivine, clinopyroxene and garnet are present for matrix melting from 6 GPa to about 3·3 GPa (Walter, 1998). The principal change is then the increasing Al content of clinopyroxene with decreasing pressure that leads to a small increase in the ratio of clinopyroxene to garnet as pressure falls. Once pressures are sufficiently low that orthopyroxene becomes a solidus phase (<3·3 GPa for M), the principal change with falling pressure is the increase in Ca content

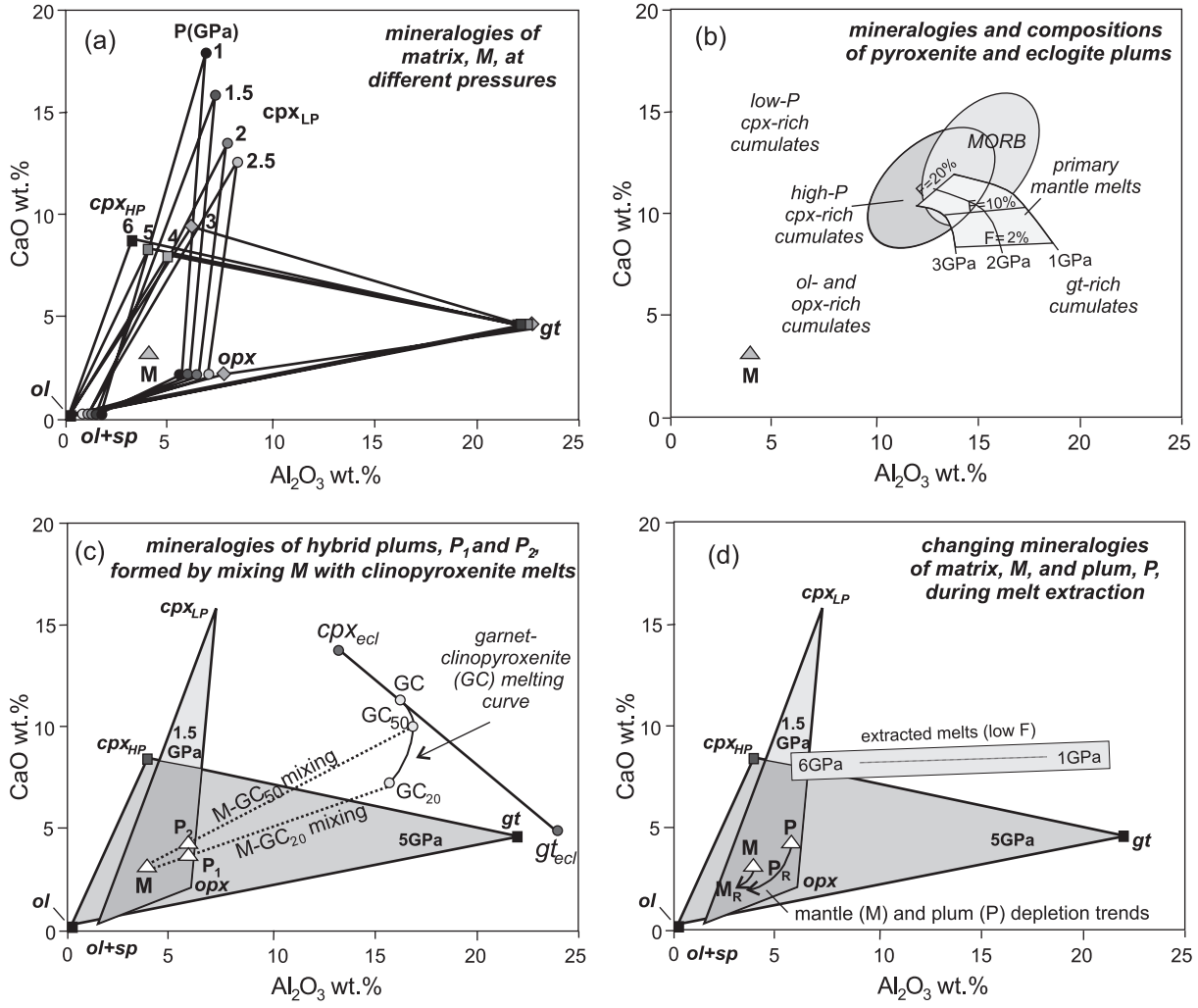

Fig. 5. Illustration of the methods used to relate mantle composition to mantle mineralogy based on CaO–Al_2O_3 covariations. (a) illustrates how the mineral proportions making up matrix mantle, M, can be tracked during decompression by using the 'centre of gravity rule' to calculate the position of M within the triangle made up by the phases stable at that pressure. The figure shows the triangles for M at pressures from 1 to 6 GPa. (b) illustrates the potential compositions of pyroxenite and eclogite plums embedded within the matrix mantle, emphasizing the wide range of possible compositions of plums of igneous origin. Plums that originated as primary basaltic melts can be assigned compositions within a grid with pressure of melt generation and degree of melting as the principal variables. MORB plums occupy a field consistent with evolution from primary melts formed by low-pressure, moderate-degree melting. Cumulate plums vary in composition according to pressure of crystallization and cumulate mineralogy. Sedimentary plums (not shown) can have a similarly wide range of composition dependent on provenance and metamorphic history. (c) illustrates how the composition of hybid mantle plums can be modelled as mixtures of matrix mantle and melts derived from one of the plums in (b), in this case garnet clinopyroxenite (GC). The figure illustrates the formation of two hybrid plums, P_1 and P_2, by mixing of matrix mantle, M, with melts formed by 20% melting (GC_{20}) and 50% melting (GC_{20}) of GC. (d) illustrates how the compositions of matrix (M) and plum (P) compositions can be tracked during melt extraction by first calculating the residual compositions (M_R and P_R), and then using the residual compositions to estimate mineral assemblages using triangles such as those for 1·5 GPa and 5 GPa. The figure also illustrates how the compositions of the melts extracted are pressure dependent (high Al at low *P* and low Al at high *P*), which must be taken into account in calculating the residual compositions.

of clinopyroxene that leads to a decrease in the proportion of clinopyroxene (and increase in proportion of orthopyroxene) as pressure falls.

When the garnet–spinel transition is reached (2·8 GPa for MORB pyrolite: Robinson & Wood, 1998), residual garnet will react with olivine to form two pyroxenes and spinel. At this pressure, both orthopyroxene and clinopyroxene have moderately Al-rich compositions. With falling pressure, the Ca content of the clinopyroxene increases, causing the proportion of clinopyroxene to decrease and the proportion of orthopyroxene to increase. At the same time, both pyroxenes become less Al-rich and the proportion of spinel increases to retain Al mass balance.

Appendix B gives the equations that allow the mass fractions of phases to be computed. Above 3·3 GPa, where only garnet, clinopyroxene and olivine are present, the equation is a straightforward manipulation of the simultaneous equations for CaO and Al_2O_3 mass balance. Between 3·3 and 2·8 GPa, however, where olivine, clinopyroxene, orthopyroxene and garnet are all present, the phase proportions have to be obtained by first estimating the mass fraction of garnet. For spinel lherzolites, at pressures <2·8 GPa, olivine, clinopyroxene, orthopyroxene and spinel are all present and the phase proportions have to be obtained by first estimating the mass fraction of spinel.

If melt is extracted at any pressure, CaO and Al_2O_3 will be lost from the asthenosphere. Before any further calculation is made of mineral proportions, new CaO and Al_2O_3 concentrations of the residue must be calculated using melt reaction coefficients. This is illustrated in Fig. 5d. The recalculation procedure is also described in Appendix C. For simplicity, the assumption made here is that melting changes the position of M but not the mineral compositions. Clearly, this is not the case, but the small fractions extracted have only a small effect on mineral composition compared with the large effects of pressure and temperature. However, more detailed modelling could be carried out by varying mineral compositions and using all the major elements in calculating phase proportions.

Tracking plum mineralogies

Tracking plum mineralogies is difficult because there are so many potential types of plum and because plum extraction may be a single-stage event (direct extraction of melt from the plum) or a two-stage event (plum-derived melt reacts with the matrix to form a hybrid peridotite, which then subsequently melts). This distinction is highly significant in modelling melt extraction: for example, the relative rates of melting of matrix and plums (r) will be much smaller for a single-stage event. In the single-stage model (Hirschmann & Stolper, 1996; Pertermann & Hirschmann, 2003), eclogite and pyroxenite plums release melt in response to decompression over a large depth range beginning some 150°C below the dry peridotite solidus. In a two-stage model (Yaxley & Green, 1998; Yaxley, 2000), the melt generated in this way reacts with the matrix to form a hybrid peridotite. Melting then takes place at the solidus of the hybrid peridotite, which is at only a slightly lower temperature than that of the matrix itself.

The variability in plum type was discussed by Pertermann & Hirschmann (2003), who demonstrated that naturally occurring eclogites and pyroxenites may occupy a large part of CaO–Al_2O_3 space. One reason for this large spread in composition is that they may have many sources, including: (1) recycled oceanic crust (basalts and gabbros); (2) recycled sedimentary materials; (3) alkali basalt veins; (4) vein-wall cumulates. The CaO and Al_2O_3 ranges of these are illustrated in Fig. 5b. Mid-ocean ridge basalt and gabbro typically have CaO and Al_2O_3 of 13 ± 3 and 15 ± 3 wt %, respectively. Alkali basalt veins that are recycled via subducted oceanic lithosphere (Niu *et al.*, 2002) or entrained within the asthenosphere during plume melting (Le Roex *et al.*, 2002) form from near-primary, low-degree melts. Thus they typically have lower CaO than MORB and so lie below the MORB field (Kushiro, 2001). Cumulates have a wide range of compositions depending on which minerals predominate. High-pressure vein cumulates, such as those of Beni Bousera (Pearson *et al.*, 1993), have slightly lower CaO and Al_2O_3 than MORB whereas low-pressure cumulates typically have low Al_2O_3 and variable CaO. Recycled volcanogenic sediments (not shown in Fig. 5b) commonly plot close to the MORB field, but pelagic sediments vary greatly according to the original proportions of carbonates (CaO rich) and clay minerals (Al_2O_3 rich).

Whatever their origin, eclogite and pyroxenite plums have solidi that, even under anhydrous conditions, lie well below the peridotite matrix solidus in the 6–1 GPa region. Most experiments indicate that plums can undergo high degrees of melting before the peridotite matrix solidus is reached. For example, Pertermann & Hirschmann (2003) estimated that plums at 3 GPa will undergo 60% of batch melting, although fractional melting would not give such a high value. Experimental melting of eclogites and pyroxenites at high temperatures and pressures consistently demonstrates that the first melts extracted contain low amounts of CaO, becoming more CaO rich as melting proceeds. The residue, in contrast, becomes more CaO rich. Garnet melts at a greater rate than clinopyroxene although the difference may be small (e.g. Yasuda *et al.*, 1994): in other words, the increasing CaO content of the plums is matched by an increasing CaO content of the residual clinopyroxene. This work makes the same assumption as Hirschmann & Stolper (1996) to model eclogite and pyroxenite plums; namely, that the process approximates to modal melting and that partition coefficients do not vary as melting proceeds. This may seem a considerable simplification, but varying the parameters has little effect on the projection modelled here. For more detailed studies, and different projections, a more detailed model may be needed.

Hybrid peridotite plums are, as defined above, the reaction or impregnation products of eclogite/pyroxenite-derived melt and the peridotite matrix. The product of eclogite or pyroxenite melting is silica-rich and so reacts with the surrounding mantle to generate a hybrid pyroxene-rich peridotite. The composition of the hybrid mantle can be calculated, or determined

graphically, by mixing of matrix and eclogite-derived melt. In the three garnet pyroxenites or eclogites for which high-pressure, anhydrous experiments have been performed (Yaxley & Green, 1998; Klemme *et al.*, 2002; Pertermann & Hirschmann, 2003), CaO increases with degree of melting, whereas Al_2O_3 varies only slightly. Figure 5c shows the garnet clinopyroxenite melting trend from the experiments of Pertermann & Hirschmann (2003), where GC is the starting composition and GC_{20} and GC_{50} are the compositions for 20 and 50% melting, respectively. Mixing lines can be drawn from mantle M to the chosen point on the melting trend and the hybrid composition calculated by mass balance using the component compositions and the chosen mass fraction of added melt.

The hybrid peridotites can be tracked in the same way as the matrix peridotites, by using the techniques illustrated in Fig. 5a. The main problem is how to estimate the mineral compositions. However, Yaxley & Green (1998) demonstrated that, if the melt:matrix ratio is low, the minerals in the hybrid mantle have very similar compositions to the minerals in the matrix and that assumption is made here. Clearly, however, a small shift to higher CaO and Al_2O_3 will take place and could be taken into account for more precise modelling.

Tracking reaction coefficients and partition coefficients for peridotites

Melt reaction coefficients are the proportions of phases contributing to the melt and are used to calculate P in the melting equations (Appendix A). The melt reaction coefficients used to model mantle preconditioning (Table 1) are those that are most applicable to near-solidus melting. Values at low pressure (1–1·5 GPa) are taken from Kinzler & Grove (1992), Baker & Stolper (1994), Walter & Presnall (1994), Robinson *et al.* (1998) and Walter (1999). Those at intermediate pressure (2–3·5 GPa) additionally incorporate values of Walter *et al.* (1995) and Walter (1999). Those at high pressure ($\geq$3·5 GPa) are based on values of Walter (1998). It should be noted that, for melt extraction at high presssure during flow in which degrees of melting are low, orthopyroxene will not be a product at the solidus; instead, it will appear as the degree of melting increases. In consequence, the orthopyroxene reaction coefficients used here are lower than those in the compilation made by Longhi (2002), because those apply to high degrees of melting (and thus a polybaric melting column) but not small amounts of melt extracted from the base of a melting column.

For the partition coefficients, the partitioning experiments of Salters & Longhi (1999) and Salters *et al.* (2002) are most directly applicable to this study. Unfortunately, they refer to temperatures that are some 100°C above both Hirschmann's (2000) and Herzberg *et al.*'s (2000) best-fit mantle solidi and do not extend to pressures beyond 3·4 GPa. However, good fits with other experimental data indicate that their parameterizations are more robust. To obtain clinopyroxene–melt and garnet–melt partition coefficients appropriate for low-degree melts of fertile mantle peridotites over the pressure range of 1–6 GPa, this paper uses the parameterizations published by Salters *et al.* (2002) and then applies them to the few experiments in which degrees of melting are within the range 2–12 wt % and for which both melt and mineral compositions are published. Figure 6 illustrates the relationship between partition coefficient and pressure at the solidus, and Table 1 gives the values used in this study for Nd and Yb. Errors (2σ) on regression lines are typically about 0·1 log units.

Table 1 shows that the bulk distribution coefficients for Nd generally decrease with increasing pressure along the anhydrous, peridotite solidus, although there is a plateau at intermediate pressures. For Yb, there is a balance between the increase in proportion of garnet with depth and the decrease in partition coefficient resulting from changes in P, T, and melt and mineral compositions. The greatest bulk partition coefficients for Nd are at shallowest depths, but the greatest values for Yb are at intermediate depth (3·5 GPa).

A key question is whether these partition coefficients are also valid at ultra-low degrees of melting, when minor hydrous phases may contribute significantly to the melt. Robinson *et al.* (1998) discovered that melt compositions for <3% melting of MORB pyrolite at 1·5 GPa have high Si and Na and low Mg and Ca, although melt compositions for low degrees of melting of the depleted Tinaquillo peridotite have 'normal' values. Parameterization of their data for experiments with 0·8–0·9 degrees of melting MORB pyrolite gives clinopyroxene–melt partition coefficients of 0·71 for Yb and 0·42 for Nd, well above the values of 0·4 for Yb and 0·18 for Nd listed in Table 1. Blundy *et al.* (1998) obtained a clinopyroxene–melt partition coefficient >1 by direct measurement on a *c.* 1% melt at the same pressure. On the other hand, the values cited in Table 1 almost exactly match the parameterizations of data obtained for 2·4 wt % melting at 1 GPa (Schwab & Johnson, 2001) and for <1 wt % melting at 5 GPa (Herzberg & Zhang, 1996). Gaetani (2004) explained that it is the first melts of fertile mantle at low pressure that give unusually high partition coefficients because the high Na and Al depolymerize the melt. These details will need to be incorporated into more sophisticated models, as will the role of water in low-degree melts. However, varying partition coefficients on this scale has little effect on the shapes of melt extraction trajectories, principally because much of the melt extraction takes place at higher pressures where Na and Al concentrations of low-degree melts are not so high.

Table 1: Data used in the melt extraction modelling

P (GPa):	1·0	1·5	2·0	2·5	3·0	3·5	4·0	4·5	5·0	5·5	6·0
T (°C):	1248	1309	1366	1421	1473	1523	1571	1615	1658	1697	1734
Mineral compositions											
CaO (cp)	18·5	16·5	14·5	12·5	10·5	7·9	8·1	8·3	8·5	8·7	8·9
CaO (gt)					4·8	4·7	4·7	4·7	4·6	4·6	4·6
CaO (op)	2·1	2·1	2·1	2·1	2·2						
CaO (ol)	0·3	0·3	0·3	0·3	0·3	0·3	0·3	0·3	0·3	0·3	0·3
CaO (sp)	0·3	0·3	0·3	0·3	0·3	0·3	0·3	0·3	0·3	0·3	0·3
Al_2O_3 (cp)	6·8	7·3	7·8	8·3	5·5	5·1	4·7	4·3	3·9	3·5	3·1
Al_2O_3 (gt)					23·0	22·8	22·6	22·4	22·2	22·0	21·8
Al_2O_3 (op)	5·5	6·0	6·5	7·0	7·5						
Al_2O_3 (ol)	0·2	0·2	0·2	0·2	0·2	0·2	0·2	0·2	0·2	0·2	0·2
Al_2O_3 (sp)	58	58	58	58	58	58	58	58	58	58	58
Matrix (M) mineralogy											
cpx	15·0	17·0	19·6	23·3	27·5	36·3	34·8	33·4	32·2	31·0	29·8
gt					2·9	10·1	11·1	12·1	13·0	13·9	14·7
opx	26·1	25·2	23·2	19·9	14·1						
ol	56·0	55·5	55·3	55·4	55·5	53·7	54·1	54·6	54·8	55·1	55·4
sp	2·9	2·4	1·9	1·4							
Hybrid plum (H) mineralogy											
cpx	18·1	21·0	24·8	30·0	36·5	49·0	46·9	45·0	43·5	41·8	40·2
gt					5·1	17·7	19·2	20·5	21·8	23·0	24·2
opx	66·5	60·7	54·2	46·4	28·9						
ol	12·4	15·9	19·1	22·1	29·6	33·3	34·0	34·5	34·8	35·2	35·6
sp	2·9	2·4	1·9	1·4							
Reaction coefficients											
cpx	0·75	0·90	1·10	1·25	0·80	0·60	0·60	0·55	0·50	0·50	0·50
gt					0·25	0·30	0·25	0·25	0·25	0·25	0·25
opx	0·45	0·20	0·00	−0·30	−0·15						
ol	−0·30	−0·20	−0·10	−0·05	0·10	0·10	0·15	0·20	0·25	0·25	0·25
sp	0·10	0·10	0·10	0·10							
melt	0·00	0·00	0·00	0·00	0·00	0·00	0·00	0·00	0·00	0·00	0·00
P(Yb)	0·48	0·42	0·39	0·34	1·33	1·29	0·92	0·77	0·64	0·54	0·45
P(Nd)	0·190	0·166	0·154	0·121	0·082	0·054	0·038	0·027	0·019	0·014	0·010
Partition coefficients (Yb)											
cpx	0·54	0·44	0·36	0·30	0·24	0·20	0·16	0·13	0·11	0·09	0·07
gt					4·6	3·9	3·3	2·8	2·4	2·0	1·7
opx	0·18	0·15	0·13	0·11	0·09						
ol	0·031	0·026	0·022	0·019	0·016	0·014	0·012	0·01	0·009	0·007	0·006
sp	0·004	0·004	0·004	0·004							
D_o(M)	0·15	0·13	0·11	0·10	0·22	0·47	0·43	0·39	0·35	0·31	0·27
D_o(H)	0·22	0·19	0·17	0·15	0·36	0·79	0·71	0·63	0·57	0·50	0·44
Partition coefficients (Nd)											
cpx	0·24	0·18	0·14	0·10	0·079	0·060	0·044	0·033	0·025	0·018	0·014
gt					0·080	0·060	0·044	0·033	0·025	0·018	0·014
opx	0·022	0·018	0·016	0·013	0·011						

P (GPa):	1·0	1·5	2·0	2·5	3·0	3·5	4·0	4·5	5·0	5·5	6·0
T (°C):	1248	1309	1366	1421	1473	1523	1571	1615	1658	1697	1734
ol	0·001	0·001	0·001	0·001	0·001	0·001	0·001	0·001	0·001	0·001	0·001
sp	0·001	0·001	0·001	0·001							
D_o(M)	0·042	0·036	0·032	0·026	0·026	0·028	0·021	0·016	0·012	0·009	0·007
D_o(H)	0·060	0·051	0·046	0·038	0·038	0·042	0·031	0·024	0·019	0·014	0·011

The calculations of bulk distribution coefficients incorporate a melt fraction, ϕ, here taken as 0·02.

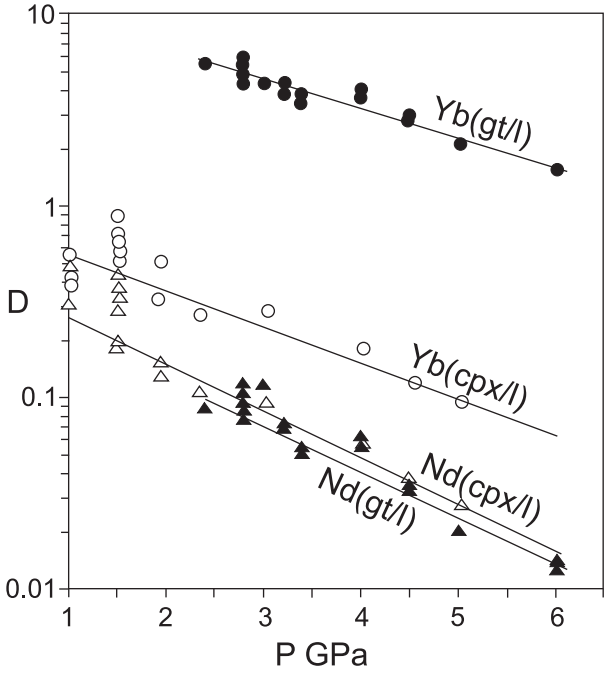

Fig. 6. Measured and calculated Nd, Yb clinopyroxene–melt and garnet–melt partition coefficients (*D*) for moderate to low (<12%) degrees of melting at 1–6 GPa. Data sources are Baker & Stolper (1994), Walter *et al.* (1995), Herzberg & Zhang (1996), Kinzler (1997), Blundy *et al.* (1998), Robinson *et al.* (1998) and Schwab & Johnson (2001).

Tracking reaction coefficients and partition coefficients for eclogites and pyroxenites

For a given clinopyroxene:garnet ratio, reaction coefficients should vary slightly with pressure down to the pressure at which garnet begins to break down, clinopyroxene entering the melt slightly faster than garnet at high pressure and garnet entering the melt slightly faster than clinopyroxene at low pressure (e.g. Yasuda *et al.*, 1994). For this paper, both minerals are assumed to contribute equally to the melt over the full range of eclogite stability. As the lower limit of garnet stability may be of the order of 1·5–2·0 GPa (Yasuda *et al.*, 1994; Hirschmann & Stolper, 1996), this eclogite mineralogy has been retained throughout melt extraction for pressures above 1·5 GPa. Studies of Beni Bousera suggest that the typical low-*P* breakdown product is a corundum-bearing websterite (Kornprobst *et al.*, 1990). However, this is unlikely to be relevant, as the plums will normally be ultra-depleted in incompatible elements through melt extraction by this stage.

For the garnet–melt partition coefficients, Hirschmann & Stolper's (1996) compilation (for $P<3$ GPa) gives $D_{Yb} = 6{\cdot}4$ [by interpolation using the approach of Wood & Blundy (1997)] and $D_{Nd} = 0{\cdot}052$, and the data of Klemme *et al.* (2002) gives (at 3 GPa) $D_{Yb} = 7{\cdot}1$ and $D_{Nd} = 0{\cdot}035$ (by interpolation). Equivalent values for clinopyroxene compilations are respectively $D_{Yb} = 0{\cdot}44$ and $D_{Nd} = 0{\cdot}187$, and $D_{Yb} = 0{\cdot}64$ and $D_{Nd} = 0{\cdot}17$. For higher pressures, the experimental data of Yasuda *et al.* (1994) at 5 GPa, parameterized according to Salters *et al.* (2002), give $D_{Yb} = 7{\cdot}9$ and $D_{Nd} = 0{\cdot}12$ for garnet, and $D_{Yb} = 0{\cdot}48$ and $D_{Nd} = 0{\cdot}186$ for clinopyroxene. These data are insufficient to indicate any pressure, composition or temperature dependence. However, the contrast between compatible Yb and incompatible Nd is so great that it masks possible errors in the individual Nd and Yb coefficients in most models. This paper uses the same values throughout: $D_{Yb} = 7{\cdot}0$ and $D_{Nd} = 0{\cdot}07$ for garnet; and $D_{Yb} = 0{\cdot}45$ and $D_{Nd} = 0{\cdot}18$ for clinopyroxene.

A note of caution is that van Westrenen *et al.* (2001) found that eclogites and garnet pyroxenites with >19 mol % Ca on the garnet X-site could have markedly different *D* values, notably higher coefficients for Nd. It is, therefore, likely that some eclogites do exhibit different partition coefficients from those used in this study although, again, the principal conclusions are not affected.

NUMERICAL EXPERIMENTS ON MANTLE PRECONDITIONING

The equations developed in this paper coupled with the values of the melting parameters listed in Table 1 allow numerical experiments on mantle preconditioning to be carried out for the plot of $^{143}Nd/^{144}Nd$ vs Yb/Nd

(I_1 vs $T_{2/1}$, where 1 indicates Nd and 2 indicates Yb). The method is first to define compositions of the matrix mantle (M) and plums (P) prior to preconditioning. Here, the matrix has arbitrary values of 1 ppm Nd, 0·4 ppm Yb and $^{143}Nd/^{144}Nd = 0{\cdot}5132$, and the plums (P) are hybrid plums (mantle metasomatized by plum melts) containing 5 ppm Nd, 0·5 ppm Yb, and $^{143}Nd/^{144}Nd = 0{\cdot}5126$. The pressure at which the mantle crosses its solidus is next defined. The matrix and plum mineralogies at this pressure are then calculated using the equations in Appendix B, and the corresponding partition and reaction coefficients calculated. The composition of the residual asthenosphere is then calculated from equations (A3) and (A4) for the chosen values of mass fraction of plums (M_P), relative rate of plum melting (r), mass fraction of trapped melt (F_T) and efficiency of melt extraction (ϕ).

It should be noted that these experiments are based on melt extraction at a single pressure. For multiple episodes of melt extraction, the mineralogy would need to be recalculated as described in Appendix C and the process repeated.

Figure 7 depicts some of the key results. It depicts models in which the variables are initially fixed at $M_P = 0{\cdot}3$, $r = 0{\cdot}1$, $F_T = 0$ (no chemical exchange between plums and matrix), plum composition P from Fig. 5d, melt extraction at 2·5 GPa throughout, and an efficiency of melt extraction (ϕ) of 0·02. The various parts of Fig. 7 then highlight the effect of varying each of the parameters in turn.

Figure 7a illustrates the effects of variable r; that is, variable rate of melting of matrix with respect to rate of melting of plums. As r decreases from unity (matrix and plums melt at equal rates) to 0·001 (almost entirely plums melting), the melt extraction trajectories become steeper and a plateau is reached at progressively lower Yb/Nd ratios. For $r = 0{\cdot}001$, when the plum component dominates melting, the extraction trend is only just to the right of the mixing line before converging on the matrix composition. This distinctive trend results because the matrix composition scarcely changes whereas the plums become progressively depleted in incompatible elements until they no longer contribute significant Nd to the bulk mantle composition. This has the interesting consequence that even apparently simple mixing trends between two end-member components could be explained by preconditioning with very low values of r.

Figure 7b illustrates the effect of variable M_P; that is, variable mass fractions of plums. Each trajectory again follows a positive slope ending in a plateau. As the mass fraction of plums decreases, the Nd contribution from the plums decreases more rapidly to 'background', and the bulk mantle composition reaches its plateau at lower ratios of Yb/Nd.

Figure 7c illustrates the effects of different plum mineralogies. The effect of mineralogy is illustrated by varying the proportion of clinopyroxene while retaining the ratio of olivine to orthopyroxene. As the mass fraction of clinopyroxene in the plums increases, the bulk distribution coefficient for Yb increases and Yb is more strongly retained in the residue from melt extraction whereas Nd is much less affected. Thus, the greater the mass fraction of clinopyroxene, the more rapid the increase in Yb/Nd ratio for a given melt loss and the shallower the melt extraction trajectory.

Figure 7d illustrates the effects of depth of melt extraction during mantle flow. At high temperatures and pressures, melt extraction begins well within the garnet lherzolite facies whereas, at lower temperatures, melt extraction begins within the spinel lherzolite facies. The consequence is flatter trends for the higher temperatures and pressures, because melting in garnet lherzolite facies causes Yb to be retained relatively strongly in the melt extraction residue. Subsequent partial melting of such a mantle source therefore yields basalts with high Yb/Nd ratios.

Figure 7e illustrates the effects of chemical exchange between plums and matrix during melt extraction. The variable is F_T, the retained melt expressed as a mass fraction of the residual mantle: the higher the value of F_T, the lower the plateau value of the Nd isotope ratio. The retained melt is treated as pooled fractional melt from the related melt extraction episode.

Figure 7f illustrates the effects of efficiency of melt extraction. The variable is ϕ, the extent of melting required before melt can be extracted from the flowing asthenosphere. The higher the value of ϕ, the less rapid the depletion of Nd in the mantle and hence the steeper the melt extraction trend and the earlier the plateau is reached.

It should be noted also that Fig. 7 is based on only two components, a MORB mantle component with high Yb/Nd and high Nd isotope ratio and a plum component with low Yb/Nd and low Nd isotope ratio. It is, as Fig. 3a demonstrates, equally possible to model other types of plum, or mixture of plums, although (as will be seen) the scenario chosen best simulates natural systems. This particular projection of $^{143}Nd/^{144}Nd$ against M/Nd (where M is any incompatible element) is sensitive not only to the composition of the plums, but also to their age and hence their residence time in the mantle. For example, Yb/Nd correlates with Sm/Yb, so the compositions of plums (and matrix) will evolve with time and the precise Nd isotope ratios will depend on both the initial isotope ratio and the residence time in the mantle before melting. This is clearly important if the plums represent old, recycled material. For example, the pyroxenite veins of Beni Bousera (Pearson *et al.*, 1993), often cited as examples of the plums in a plum-pudding mantle, have very high Yb/Nd ratios but low Nd isotope ratios. They could melt to produce magma with low Yb/Nd ratios, which would

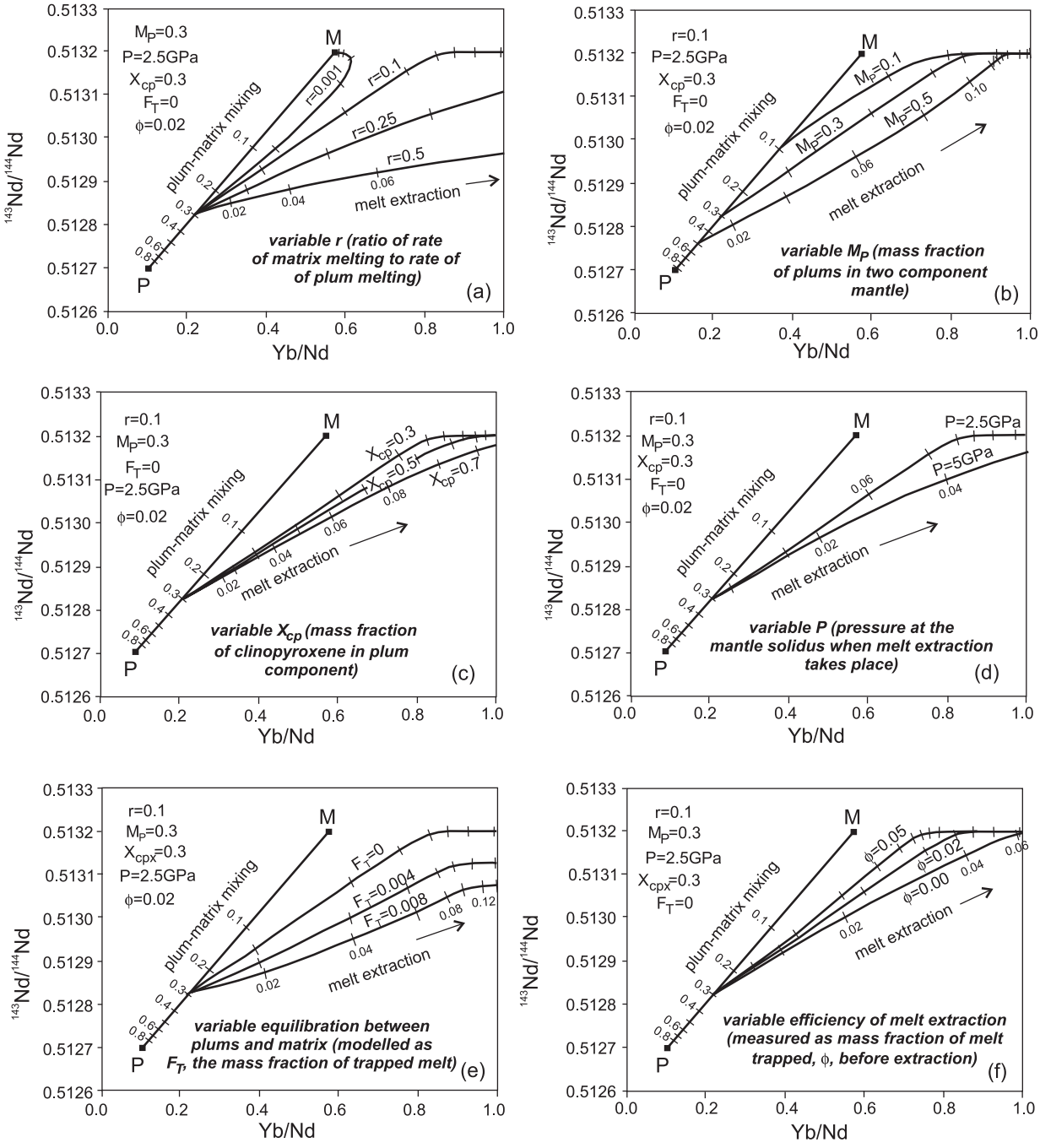

Fig. 7. Numerical experiments in melt extraction during mantle flow, illustrating the effects of varying: (a) relative rate of matrix and plum melting; (b) mass fraction of plums; (c) plum mineralogy; (d) pressure and temperature; (e) chemical exchange between plums and matrix; (f) efficiency of melt extraction. The experiments show that each parameter can influence melt extraction trajectories, with shallower trends favoured by high values of r, M_P, X_{cpx}, P and F_T, and low values of ϕ. The typical melt extraction trajectory is at a shallower angle than the trend formed by mixing matrix and plums in the starting 'plum pudding' mantle composition. It is close to linear while both matrix and plums contribute Nd to the melt budget, eventually reaching a plateau once the Nd in the plums has reached sufficiently low levels that the plums no longer contribute to the melt budget.

react with mantle to yield hybrid plums of the required composition. However, if recycled through the Earth, the veins would rapidly evolve to very high Nd isotope ratios and therefore represent unsuitable compositions.

Overall, therefore, the numerical experiments demonstrate that melt extraction trajectories differ from mixing trends in both the gradient of plum removal and the presence of a plateau. The gradient becomes increasingly

shallow (and increasingly divergent from a mixing gradient) for higher pressures and temperatures of melt extraction, for lower rates of plum melting compared with matrix melting, for plums with high proportions of garnet and clinopyroxene, for high proportions of plums relative to matrix and for efficient melt extraction. The position of the plateau depends on the isotope composition of the matrix, the extent of chemical exchange between plums and matrix, and the isotope composition of the plums. Moreover, although the overall trajectories do not resemble mixing lines, almost all lavas are derived from mantle with Yb/Nd <0·8. Most of the modelled trajectories are close to linear over this range. Thus, it cannot be assumed without further evaluation that linear trends on this type of plot must result from source mixing, as melt extraction could give the same outcome.

SOME POSSIBLE EXAMPLES OF MANTLE PRECONDITIONING

There are many examples that could be used for comparison with the theoretical models. For reasons of space, this paper focuses on the one projection of $^{143}Nd/^{144}Nd$ against Yb/Nd and three areas: one representative of possible preconditioning in a back-arc setting, one representative of possible preconditioning during continental break-up, and one representative of possible preconditioning during plume–ridge interaction. In all examples, isotope data have been normalized to La Jolla of 0·511858 or BCR-1 of 0·512643. Where standard data have been reported, trace element data are normalized to recommended values.

Preconditioning by mantle flow into an arc–basin system: Bouvet–Scotia Sea

The compositional relationships between lavas from the South American Antarctic Ridge (SAAR), East Scotia Ridge (ESR) back-arc spreading centre and South Sandwich Islands (SSI) island arc (Fig. 8) provide a good test of the models presented here. Pearce *et al.* (1995) have already demonstrated that the depleted nature of the South Sandwich arc lavas supports the hypothesis of McCulloch & Gamble (1991) and Woodhead *et al.* (1993) that the mantle reaching the arc front has been preconditioned by melt loss in the back-arc. Leat *et al.* (2000, 2004) and Fretzdorff *et al.* (2002) additionally found that lavas at the edges of the basin were more enriched in incompatible elements than those in the centre and so supported models for flow of enriched mantle into the back-arc from both north and south. Pearce *et al.* (2001) further demonstrated that the lavas from the East Scotia Ridge form trends in isotope space that point towards the composition of Bouvet Island; thus they belong to the Bouvet mantle domain,

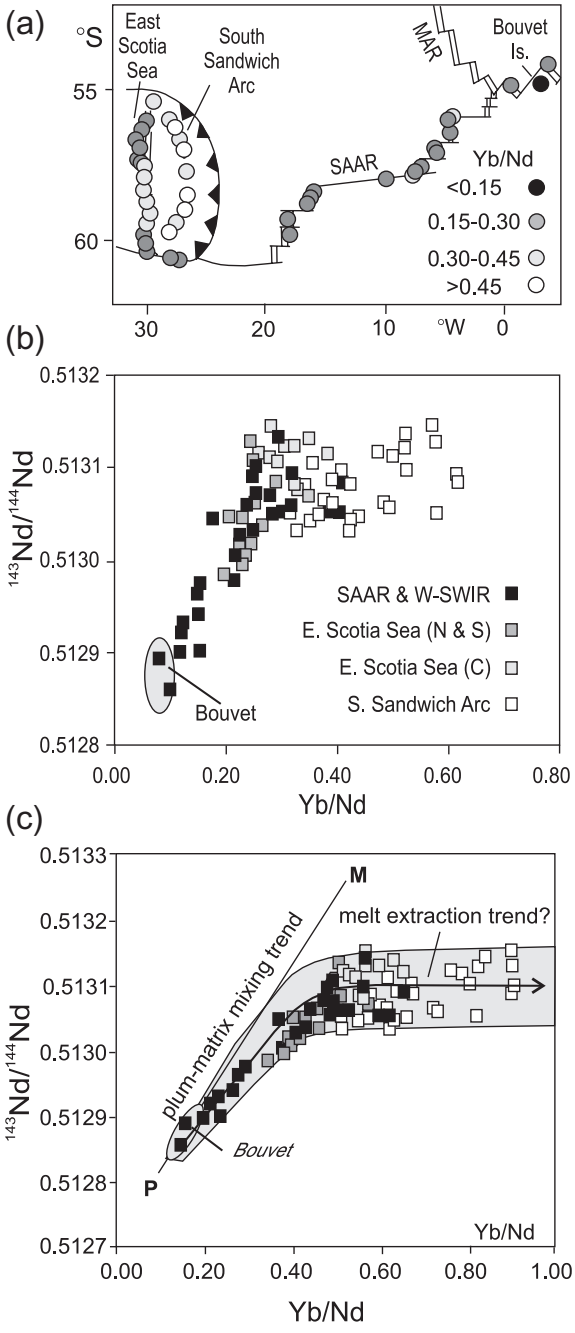

Fig. 8. A possible example of mantle preconditioning involving a subduction system. (a) Yb/Nd geochemical map of the region between Bouvet Island and the Scotia arc–basin system showing a chemical gradient formed by increasing Yb/Nd from the Bouvet plume to the arc front. (b) Plot of $^{143}Nd/^{144}Nd$ against Yb/Nd for the lavas (SAAR, South America–Antarctic Ridge; SWIR, South-West Indian Ridge. (c) Plot of $^{143}Nd/^{144}Nd$ against Yb/Nd for the mantle using inverted data from (b) assuming 15% pooled melting for the ridge lavas and 20% melting for the arc lavas (M, matrix; P, plums). Comparison with the numerical experiments indicates that the trend in (c) could be explained at least in part by preconditioning of incompatible element-enriched mantle containing plums from the Bouvet plume flowing into the arc–basin system towards the arc front (see Fig. 1b). Data are taken from the sources cited in the text.

which includes the SAAR, the southernmost Mid-Atlantic Ridge and the western part of the South-West Indian Ridge. A. P. Le Roex *et al.* (1983, 1985) and P. J. Le Roex *et al.* (2002) explained the Bouvet mantle domain in terms of dispersion of mantle that has been both depleted and variably veined by small-degree melts during upwelling of the plume.

Figure 8a shows the extent of the regional geochemical gradient using Yb/Nd as an example. Yb/Nd ratios vary from a low value at Bouvet Island through moderately low values along the SAAR and edges of the ESR to high and ultra-high values at the arc front. It should be noted that the arc data have been corrected for the fact that some 20% of Nd in their sources has a mixed subducted crust and sediment derivation as recognized and quantified by Pearce *et al.* (1995).

Figure 8b shows the plot of $^{143}Nd/^{144}Nd$ against Yb/Nd. The SAAR and ESR margins form a steep linear trend that ends as a small plateau. The arc almost entirely forms a flat trend or plateau at approximately the same Nd isotope ratio as the ridges. There is a significant spread in the arc data, but this may be due to errors in the subduction correction and variations in degree of melting. Neither is, however, of sufficient magnitude to negate the fact that the overall shape of the trajectory (diagonal trend, then plateau) resembles that obtained by the numerical experiments in Fig. 7.

Figure 8c gives the trajectory expressed in terms of mantle compositions. Inversion of the lava data to the composition of its mantle source was carried out as illustrated in Fig. 4b by assuming an average 15% pooled fractional melting for each ridge composition and 20% for the arc compositions. The mantle then follows a steep trend finishing with a plateau at a Yb/Nd ratio of 0·5 and $^{143}Nd/^{144}Nd$ ratio of 0·51305–0·51315. This trajectory resembles the outcome of numerical experiments on mantle preconditioning for small values of r, small values of M_P, low mantle temperatures, high ϕ, or combinations of these (Fig. 7). Preconditioning is not, however, the only possible explanation. The trajectory could be explained by three-component mixing [a plum component, and depleted MORB mantle (DMM) component and an ultra-depleted component], although this is unlikely given its linear arrays in isotope space (Kurz *et al.*, 1998). Alternatively, the first part of the trajectory could be explained by two-component mixing and the plateau by preconditioning or by dynamic melting of the most depleted part of the mixing trend.

A further constraint has been provided by Snow *et al.* (1994) and Salters & Dick (2002). They found that the clinopyroxenes in peridotites from 10–16°E on the South-West Indian Ridge (within the Bouvet domain) are heterogeneous isotopically and include samples with higher $^{143}Nd/^{144}Nd$ than any of the apparently cogenetic lavas. Many ratios in the peridotites exceed 0·5133, significantly greater than the top of the 'plateau' formed by the lavas, which lies at about 0·51315. Their explanation is that the peridotites could be the product of partial melting of heterogeneous mantle in which the plums preferentially contribute to the pooled melts as represented by the lavas, whereas the depleted matrix contributes preferentially to the residual peridotites. If so, their high values could define the isotope ratios of the matrix in a preconditioning model. In Fig. 8c, the matrix has been placed at $^{143}Nd/^{144}Nd = 0{\cdot}51325$ and Yb/Nd = 0·56 (the approximate Yb/Nd ratio in DMM: Salters & Stracke, 2004). Any preconditioning model would then require a mixture of DMM and Bouvet plume-enriched component undergoing melt extraction during flow, with some chemical exchange between components by melt impregnation—very similar to the model proposed by Le Roex *et al.* (2002). The plums would then eventually become so depleted in Nd that they cease to contribute to the chemical budget and the mantle behaves isotopically as if it is homogeneous. Any further preconditioning (including that in the back-arc) then leads to a flat trajectory.

Preconditioning during continental break-up: Red Sea and Gulf of Tadjoura

The geochemistry of the Afar–Red Sea–Gulf of Aden region provides a test of the preconditioning models for plume-driven continental separation. The hypothesis to be tested is that asthenosphere flows from the Afar plume and is channelled between the separating African and Arabian continental lithosphere such that mantle reaching the northern part of the Red Sea and western part of the Gulf of Aden has experienced preconditioning during along-axis flow from the Afar plume.

Schilling *et al.* (1992) provided isotopic evidence for a three-component mantle mixing model for the region, their components being sub-continental mantle lithosphere, plume mantle (the 'torus part of the plume') and depleted asthenosphere. Continental crust may also be involved (Barrat *et al.*, 1993), but not for the samples used here. Altherr *et al.* (1990), Barrat *et al.* (1990) and Schilling *et al.* (1992) agreed that the lavas from the axial trough of the Red Sea and the Gulf of Aden have no sub-continental lithosphere component and so can be explained by binary mixing of a plume and depleted asthenosphere component. Altherr *et al.* (1988, 1990) did, however, question whether the lava data can be explained by a source containing variable proportions of the mantle components. They presented an alternative model of partial melting of a single heterogeneous source, in which less melting in the south leads to preferential melting of the 'low temperature fusible component'.

The geochemical map in Fig. 9a illustrates the regional geochemical variations using Yb/Nd as a tracer. Clearly,

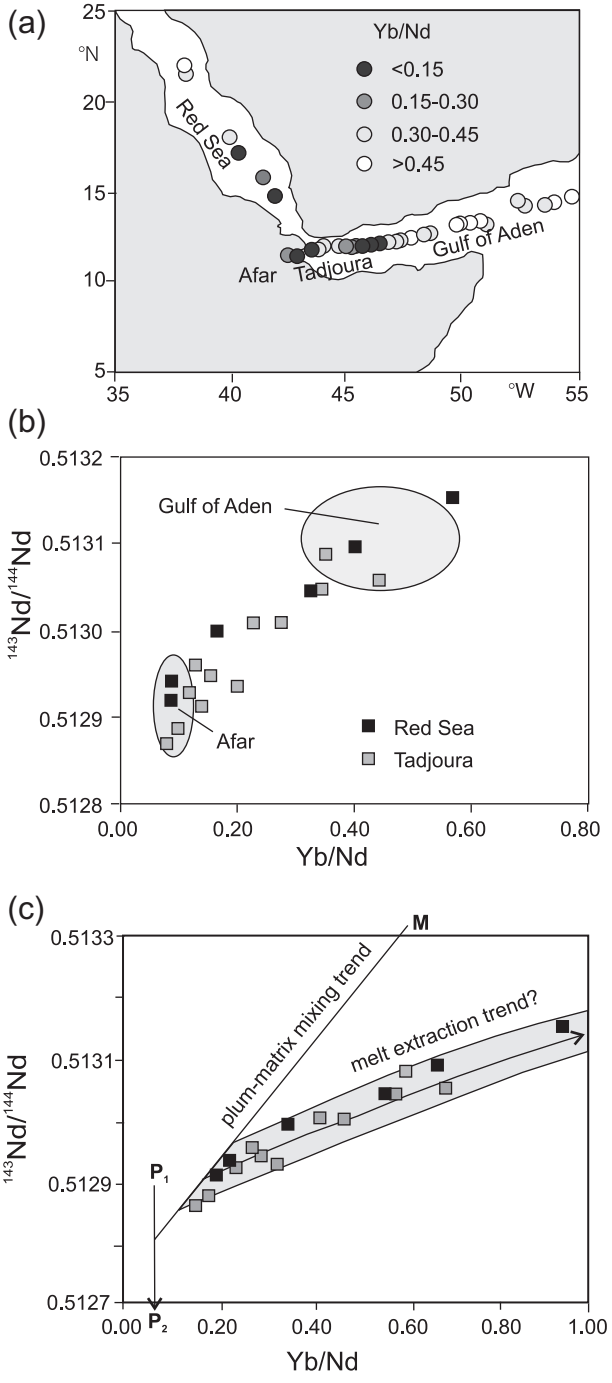

Fig. 9. A possible example of mantle preconditioning involving continental break-up. (a) Yb/Nd geochemical map of the Afar–Red Sea–Gulf of Aden region showing a chemical gradient of increasing depletion from the Afar plume along the ocean ridges. (b) Plot of $^{143}Nd/^{144}Nd$ against Yb/Nd for the Red Sea and Tadjoura lavas. (c) Plot of $^{143}Nd/^{144}Nd$ against Yb/Nd for the Red Sea and Tadjoura mantle using inverted data from (b) assuming 15% pooled melting (M, matrix; P_1 and P_2, plums). Comparison with the numerical experiments indicate that the trend in (c) could be explained at least in part by preconditioning of Afar plume mantle as it flows into the new spreading centres of the Red Sea and Gulf of Tadjoura (similar to Fig. 1c). Data are taken from the sources cited in the text.

there is a geochemical gradient away from Afar with the most distal parts of the Red Sea and Gulf of Aden having the highest ratios (i.e. being derived from the most depleted mantle). Closer to Afar, there are 'spikes' of low ratios with higher ratios between, as depicted in geochemical profiles by Schilling *et al.* (1992). In the Gulf of Aden, the effect of these spikes ends at about 48°E; further east, lavas are all depleted in incompatible elements.

The plot of $^{143}Nd/^{144}Nd$ against Yb/Nd in Fig. 9b contains two main sets of data: from the Red Sea alongstrike transect of Barrat *et al.* (1990); the Gulf of Tadjoura, Tadjoura Trough and Gulf of Aden west of 48°E, here labelled 'Tadjoura' (Schilling *et al.*, 1992) and the Gulf of Aden east of 48°E (also Schilling *et al.*, 1992). Both the Red Sea and Tadjoura samples form significant linear arrays emanating from the field of Afar data. The Gulf of Aden samples east of 48°E form a diffuse field at high Nd isotope ratios and cannot uniquely be related to the Afar plume. Particularly significant are the Red Sea data. Barrat *et al.* (1990) emphasized that they follow a clear linear trend in which the position on the trend is a function of geographical location. Samples from the south plot closer to Afar plume compositions whereas those from the north have high Yb/Nd (and low Th/Nd and La/Nd) ratios. This geographical variation was first recognized by Schilling (1973) from REE data only and he attributed it to mixing of Afar plume mantle in the south with DMM in the north.

Inversion of the data to mantle compositions assuming 15% pooled fractional melting gives the plot in Fig. 9c. Essentially, the Red Sea and Tadjoura datasets form similar linear trends at a shallower angle than the lava trends in Fig. 9b. The competing hypotheses are, therefore: (1) that these represent a mixing trend; (2) that these represent a melt extraction trajectory linked to mantle flow. In their comprehensive study, Schilling *et al.* (1992) defined the Nd isotope ratios of their three end-members as: 0·51335 for the depleted asthenosphere; 0·512907 for the plume asthenosphere; 0·5121 for the sub-continental mantle lithosphere. If we take the depleted lithosphere as having a depleted MORB mantle Yb/Nd ratio of about 0·6, and the two enriched components as having low Yb/Nd ratios, we obtain the three component compositions (M, P_1, P_2) marked in Fig. 9c. It is therefore apparent that, although the three-component mixing model works well isotopically, the observed trend extends outside the triangle formed by these components in isotope–trace element space. There are several explanations. Either the depleted asthenosphere end-member is ultra-depleted in incompatible elements (and not therefore an N-MORB source at all), or some of the variation is due to dynamic melting and not source mixing, or mantle preconditioning is an important process.

Any preconditioning model for the Red Sea must have the mantle releasing its fusible components in the south,

as Alterr *et al.* (1990) proposed, but will then require that mantle preconditioned by loss of small melt fractions during this melting event flows north to act as the source for lavas from the central part of the Red Sea. As the numerical experiments demonstrate, the Nd isotope ratio reaches a plateau only if temperatures are low enough, if the 'plums' are in a low proportion, or if the rate of plum melting is high compared with the rate of matrix melting. For hot, plume-proximal mantle, the plateau is unlikely to be reached and a linear trend is thus more likely. Thus a preconditioning model can explain the observations without requiring an unusual depleted component and merits further testing.

Preconditioning during plume–ridge interaction: Azores–Mid-Atlantic Ridge

The geochemistry of the Azores and the adjacent part of the Mid-Atlantic Ridge (MAR) provides a test of the role of mantle preconditioning during oceanic plume–ridge interaction. The comprehensive geochemical study of Yu *et al.* (1997) influenced this choice of area. Significantly, they found two distinct trends in the data and found that mixing failed to provide a simple explanation. They attributed the two Azores trends to flow of two different members of a 'family of plumes' or to one or more blobs detached from a single plume. They inferred that 'the plume-derived material reaching the MAR axis at these latitudes would be residual in nature as a result of an early removal of small melt fractions'. This is essentially the same preconditioning model as that advocated in this paper.

Figure 10a is a Yb/Nd map of the area of interest. It highlights, as low Yb/Nd ratios, the three main geochemical spikes identified by Yu *et al.* (1997), at 43°N, 39–40°N and 35°N. Between these spikes are higher values. Yu *et al.* (1997) found that only the first two of these spikes could be attributed isotopically to the Azores plume, and that they formed two trends, one for lavas north of 40·5°N and the other for lavas south of 40·5°N. Figure 10b shows these data on the plot of $^{143}Nd/^{144}Nd$ against Yb/Nd. In support of the Yu *et al.* (1997) interpretation, the data form two distinct, sub-parallel linear trends, both emanating from the Azores compositional field (e.g. Widom *et al.*, 1997). The points south of the Azores are displaced to higher Nd isotope ratios. It is thus apparent why a melt extraction mechanism, rather than mixing, has been invoked. Mixing would require two distinct enriched end-members and two distinct depleted end-members, with the enriched and depleted end-members coincidentally displaced from each other in the same direction. This is possible, but one would expect mixing lines between two enriched compositions and a single ambient, depleted mantle; that is, mixing trends should converge. By contrast, melt extraction trends for two distinct plum

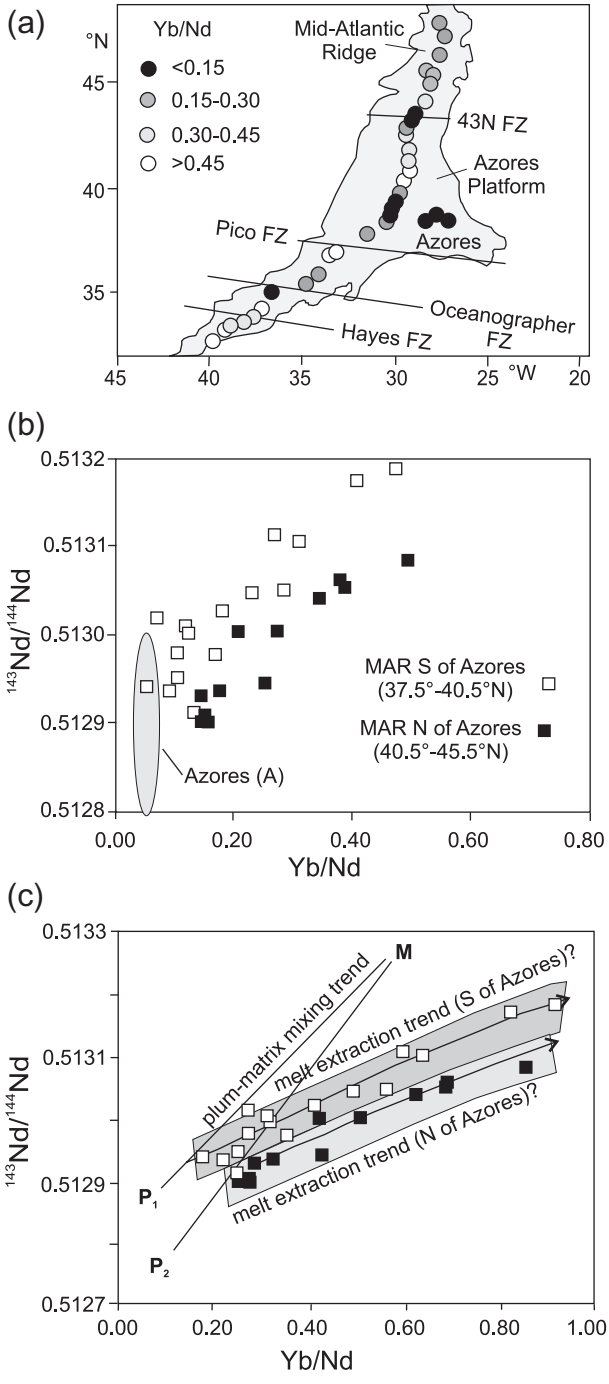

Fig. 10. (a) A possible example of mantle preconditioning involving oceanic plume–ridge interaction. (a) Yb/Nd geochemical map of the Azores–Mid-Atlantic Ridge region showing a chemical gradient from the Azores plume along the ocean ridges. (b) Plot of $^{143}Nd/^{144}Nd$ vs Yb/Nd for the Azores and Mid-Atlantic Ridge lavas. (c) Plot of $^{143}Nd/^{144}Nd$ vs Yb/Nd for the Azores and adjacent Mid-Atlantic Ridge mantle using inverted data from (b) assuming 15% pooled melting (M, matrix; P_1 and P_2, plums). Comparison with the numerical experiments indicates that the trend in (c) could be explained at least in part by preconditioning of Azores plume mantle as it flows towards and along the Mid-Atlantic Ridge (similar to Fig. 1c and d). Data are taken from the sources cited in the text.

compositions within an identical depleted matrix will produce the observed sub-parallel trends provided the plums are, as expected, melting significantly faster than the matrix (see Fig. 7b).

Figure 10c shows the lava datasets inverted to mantle compositions assuming 15% pooled fractional melting. The resulting trajectories have a shallow slope, very similar to that exhibited by the Red Sea–Afar data in Fig. 9c but shallower than the Bouvet–SAAR trajectory in Fig. 8c. These trajectories are similar to those obtained in the numerical experiments for high-pressure melt extraction, high M_P, high r, low ϕ, and combinations of these. They are also linear and thus consistent with mixing. However, mixing requires Yb/Nd to be significantly higher than the value estimated for DMM. Again, therefore, mixing does not explain the observations well (despite the linear trend), and preconditioning may provide a better model.

CONCLUSIONS

(1) Preconditioning of multi-component mantle (matrix plus plums) may be modelled using mass balance equations, as first proposed by Phipps Morgan (1999). Modelling may be made more detailed by incorporating as variables: (a) the relative rate of melting of matrix and plums; (b) mantle temperature and composition (incorporating P–T–X-dependent mantle mineralogies and partition coefficients); (c) plum composition; (d) chemical exchange between plums and matrix; (e) efficiency of melt extraction.

(2) Numerical experiments for an example of geochemical space ($^{144}Nd/^{143}Nd$–Yb/Nd) show that melt extraction trajectories exhibit both similarities and differences compared with mixing trends. They can also be linear (or close to linear) in part, but they tend to end in a plateau once the plums become so depleted in Nd that they make no effective contribution to the total Nd budget.

(3) The gradient of the near-linear part of the melt extraction trajectories in $^{144}Nd/^{143}Nd$–Yb/Nd space vary according to a series of factors. The shallowest slopes are achieved for high temperatures and pressures of melt extraction, high proportions of plums, low values of r (relatively high rates of matrix melting), and low ϕ (efficient melt extraction). The $^{144}Nd/^{143}Nd$ ratio at which the plateau is reached depends on the isotope compositions of the components and the extent of chemical exchange between them.

(4) The composition of the plums is an important factor. It is particularly important to know whether the plums lose melt directly during preconditioning (in which case r should be very low) or whether melt released from the plums first produces a hybrid mantle, which then experiences melt extraction much closer to the dry mantle solidus. The fact that observed trends are shallow implies that, if these are melt extraction trajectories, then hybrid plums better fit the isotope–trace element ratio systematics.

(5) In modelling melt extraction trajectories, it is important to use partition coefficients and mantle mineralogies appropriate for the temperature and pressure at the point at which the geotherm intersects the solidus. This can be achieved by tracking mineralogies and feeding the results into parameterized equations for the partition coefficients.

(6) Partial fusion of multi-component mantle in a melting column gives a similar mantle trajectory to that produced by preconditioning. However, the melt extracted may exhibit a much smaller variation in Nd isotope ratio if there is efficient pooling of melt fractions.

(7) Natural trajectories for examples of an arc and back-arc basin system (Bouvet–Scotia), continental break-up (Afar–Red Sea) and plume–ridge interaction (Azores) are similar to theoretical trajectories although they vary considerably from region to region. Although mixing certainly contributes to the dispersions, the range of gradients, the lack of convergence and the presence of the plateaux indicate that preconditioning of the mantle reaching the ridge or arc front could contribute significantly to the trajectories.

It is important to emphasize that this work does not claim that preconditioning is the only process operating. In any given example, mixing may prove as or more important. However, the work presented here does show that the concept of melt extraction during flow also has the ability to explain the geochemical variability in mantle sources in many different tectonic settings. There are many commonly used geochemical projections, not shown here for lack of space, where melt extraction could explain dispersions currently interpreted in other ways. The physics of melting and melt extraction are also important considerations. Preconditioning in the back-arc is widely regarded from both physical and geochemical perspectives as playing an important part in magma genesis in island arcs. The same processes of mantle flow and decompression also apply to mantle flow in the major oceans, so preconditioning of mantle should also make an important contribution to magma genesis at mid-ocean ridges and elsewhere.

ACKNOWLEDGEMENTS

This work was stimulated by discussions with Jason Phipps Morgan and Jason Morgan during visits to GEOMAR. It represents a theoretical contribution to NERC (GST/02/2792) and Antarctic Funding Initiative (NER/G/S/2000/00587) projects on the geochemistry of mantle flow in the South Atlantic and SW Pacific, and I thank

collaborators in these projects (Pamela Kempton, Phil Leat, Ian Millar, Peter Barker, Tiffany Barry, Sarah Acland and Jim Gill) for their help. I also thank Vince Salters and Michael Bizimis for advice with the partitioning studies, and Huw Davies, Yaoling Niu and Mike O'Hara for discussions in Cardiff. A number of other scientists have provided advice and/or criticism on different parts of the text, including Leonid Danyushevsky, Rex Taylor, Bramley Murton, Jon Blundy, Glenn Gaetani, Doug Wiens and Dan McKenzie. I am grateful to Tim Elliott, Marc Hirschmann, Matthew Thirlwall and Jason Phipps Morgan for their constructive reviews of the manuscript, and to Gareth Davies for his editorial contribution. Some data used in the paper were provided through a Joint Infrastructure Fund (NER/H/S/2000/00862) grant for analytical equipment.

REFERENCES

Allègre, C. J. & Turcotte, D. L. (1986). Implications of a two-component marble-cake mantle. *Nature* **323**, 123–127.

Altherr, R., Henjes-Kunst, F. & Baumann, A. (1988). Volcanic activity in the Red Sea axial trough—evidence for a large mantle diapir? *Tectonophysics* **150**, 121–133.

Altherr, R., Henjes-Kunst, F. & Baumann, A. (1990). Asthenosphere versus lithosphere as possible sources for basaltic magmas erupted during formation of the Red Sea: constraints from Sr, Pb and Nd isotopes. *Earth and Planetary Science Letters* **96**, 269–286.

Baker, M. B. & Stolper, E. M. (1994). Determination of high pressure melts using diamond aggregates. *Geochimica et Cosmochimica Acta* **58**, 2811–2827.

Barrat, J. A., Jahn, B. M., Joron, J.-L., Auvray, B. & Hamdi, H. (1990). Mantle heterogeneity in southeastern Africa: evidence from Nd isotopic compositions and hygromagmaphile element geochemistry of basaltic rocks from the Gulf of Tadjoura and southern Red Sea regions. *Earth and Planetary Science Letters* **101**, 233–247.

Barrat, J. A., Jahn, B. M., Fourcade, S. & Joron, J. L. (1993). Magma genesis in an ongoing rift zone: the Tadjoura Gulf (Afar area). *Geochimica et Cosmochimica Acta* **57**, 2291–2302.

Blundy, J. D., Robinson, J. A. C. & Wood, B. J. (1998). Heavy REE are compatible in clinopyroxene on the spinel lherzolite solidus. *Earth and Planetary Science Letters* **160**, 493–504.

Davies, J. H. & Stevenson, D. J. (1992). Physical model of source region of subduction zone volcanics. *Journal of Geophysical Research* **97**, 2037–2070.

Douglass, J., Schilling, J.-G. & Fontignie, D. (1999). Plume–ridge interactions of the Discovery and Shona mantle plumes with the southern Mid-Atlantic Ridge (40°–55°S). *Journal of Geophysical Research* **104**, 2941–2962.

Dvorkin, J., Nur, A., Mavko, G. & Ben-Avraham, Z. (1993). Narrow subducting slabs and the origin of backarc basins. *Tectonophysics* **227**, 63–79.

Elliott, T. R., Hawkesworth, C. J. & Grönvold, K. (1991). Dynamic melting of the Iceland plume. *Nature* **351**, 201–206.

Fretzdorff, S., Livermore, R. A., Devey, C. W., Leat, P. T. & Stoffers, P. (2002). Petrogenesis of the back-arc East Scotia Ridge, South Atlantic Ocean. *Journal of Petrology* **43**, 1435–1467.

Gaetani, G. A. (2004). The influence of melt structure on trace element partitioning near the peridotite solidus. *Contributions to Mineralogy and Petrology* **147**, 511–527.

Haase, K. M. (2002). Geochemical constraints on magma sources and mixing processes in Easter Microplate MORB (SE Pacific): a case study of plume–ridge interaction. *Chemical Geology* **182**, 335–355.

Haase, K. M. & Devey, C. W. (1996). Geochemistry of lavas from the Ahu and Tupa volcanic fields, Easter Hotspot, southeast Pacific: implications for intraplate magma genesis near a spreading axis. *Earth and Planetary Science Letters* **137**, 129–143.

Harpp, K. S. & White, W. M. (2001). Tracing a mantle plume: isotopic and trace element variations of Galapagos seamounts. *Geochemistry, Geophysics, Geosystems* **2**, paper number 2000GC000370.

Herzberg, C. & Zhang, J. (1996). Melting experiments on anhydrous peridotite KLB-1: compositions of magmas in the upper mantle and transition zone. *Journal of Geophysical Research* **101**, 8271–8295.

Herzberg, C., Raterron, P. & Zhang, J. (2000). New experimental observations on the anhydrous solidus for peridotite KLB-1. *Geochemistry, Geophysics, Geosystems* **2**, paper number 2000GC000089.

Hirschmann, M. M. (2000). Mantle solidus: experimental constraints and the effects of peridotite composition. *Geochemistry, Geophysics, Geosystems* **1**, paper number 2000GC000070.

Hirschmann, M. M. & Stolper, E. M. (1996). A possible role for garnet pyroxenite in the origin of the 'garnet signature' in MORB. *Contributions to Mineralogy and Petrology* **124**, 185–208.

Kincaid, C. & Hall, P. S. (2003). Role of back-arc spreading in circulation and melting at subduction zones. *Journal of Geophysical Research* **108**(B5), paper number 2001JB001174.

Kinzler, R. J. (1997). Melting of mantle peridotite at pressures approaching the spinel to garnet transition: application to mid-ocean ridge basalt petrogenesis. *Journal of Geophysical Research* **102**, 853–874.

Kinzler, R. J. & Grove, T. L. (1992). Primary magmas of mid-ocean ridge basalts. 1. Experiments and methods. *Journal of Geophysical Research* **97**, 6907–6926.

Klemme, S., Blundy, J. D. & Wood, B. J. (2002). Experimental constraints on major and trace element partitioning during partial melting of eclogite. *Geochimica et Cosmochimica Acta* **66**, 3109–3123.

Kogiso, T., Hirschmann, M. M. & Reiners, P. W. (2004). Length scales of mantle heterogeneities and their relationship to ocean island basalt geochemistry. *Geochimica et Cosmochimica Acta* **68**, 345–360.

Kornprobst, J., Piboule, M., Roden, M. & Tabit, A. (1990). Corundum-bearing garnet clinopyroxenites at Beni Bousera (Morocco): original plagioclase-rich gabbros recrystallised at depth within the mantle. *Journal of Petrology* **31**, 717–745.

Kurz, M. D., Le Roex, A. P. & Dick, H. B. J. (1998). Isotope geochemistry of the oceanic mantle near the Bouvet triple junction. *Geochimica et Cosmochimica Acta* **62**, 841–852.

Kushiro, I. (2001). Partial melting experiments on peridotite and origin of mid-ocean ridge basalt. *Annual Review of Earth and Planetary Sciences* **29**, 71–107.

Langmuir, C. H., Vocke, R. D., Hanson, G. N. & Hart, S. R. (1977). A general mixing equation applied to the petrogenesis of basalts from Iceland and Reykjanes Ridge. *Earth and Planetary Science Letters* **37**, 380–392.

Leat, P. T., Livermore, R A., Millar, I. L. & Pearce, J. A. (2000). Magma supply in back-arc spreading centre segment E2, East Scotia Ridge. *Journal of Petrology* **41**, 845–866.

Leat, P. T., Pearce, J. A., Barker, P. F., Millar, I. L., Barry, T. L. & Larter, R. D. (2004). Magma genesis and mantle flow at a subducting slab edge: the South Sandwich arc–basin system. *Earth and Planetary Science Letters* **227**, 17–35.

Le Roex, A. P., Dick, H. B. J., Erlank, A. J., Reid, A. M., Frey, F. A. & Hart, S. R. (1983). Geochemistry, mineralogy and petrogenesis of lavas erupted along the Southwest Indian Ridge between the Bouvet triple junction and 11 degrees East. *Journal of Petrology* **24**, 267–318.

Le Roex, A. P., Dick, H. B. J., Reid, A. M., Frey, F. A., Erlank, A. J. & Hart, S. R. (1985). Petrology and geochemistry of basalts from the American–Antarctic Ridge, Southern Ocean: implications for the westward influence of the Bouvet mantle plume. *Contributions to Mineralogy and Petrology* **90**, 367–380.

Le Roex, P. J., Le Roex, A. P. & Schilling, J.-G. (2002). MORB melting processes beneath the southern Mid-Atlantic Ridge (40–55S): a role for mantle plume-derived pyroxenite. *Contributions to Mineralogy and Petrology* **144**, 206–229.

Longhi, J. (2002). Some phase equilibrium systematics of lherzolite melting, 1. *Geochemistry, Geophysics, Geosystems* **3**, paper number 2001GC000204.

McCulloch, M. T. & Gamble, J. A. (1991). Geochemical and geodynamical constraints on subduction zone magmatism. *Earth and Planetary Science Letters* **102**, 358–374.

Murton, B. J., Taylor, R. N. & Thirlwall, M. F. (2002). Plume–ridge interaction: a geochemical perspective from the Reykjanes Ridge. *Journal of Petrology* **43**, 1987–2012.

Niu, Y., Collerson, K. D., Batiza, R., Wendt, I. & Regelous, M. (1999). The origin of E-type MORB at ridges far from mantle plumes: the East Pacific Rise at 11°20′N. *Journal of Geophysical Research* **104**, 7067–7087.

Niu, Y., Regelous, M., Wendt, I. J., Batiza, R. & O'Hara, M. J. (2002). Geochemistry of near-EPR seamounts: importance of source vs. process and the origin of enriched mantle component. *Earth and Planetary Science Letters* **199**, 327–345.

Pan, Y. & Batiza, R. (1998). Major element chemistry of volcanic glasses from the Easter Seamount Chain: constraints on melting conditions in the plume channel. *Journal of Geophysical Research* **103**, 5287–5304.

Pearce, J. A., Baker, P. E., Harvey, P. K. & Luff, I. W. (1995). Geochemical evidence for subduction fluxes, mantle melting and fractional crystallization beneath the South Sandwich island arc. *Journal of Petrology* **36**, 1073–1109.

Pearce, J. A., Leat, P. T., Barker, P. F. & Millar, I. L. (2001). Geochemical tracing of Pacific–Atlantic upper mantle flow through the Drake Passage. *Nature* **410**, 457–461.

Pearson, D. G., Davies, G. R. & Nixon, P. H. (1993). Geochemical constraints on the petrogenesis of diamond facies pyroxenites from the Beni Bousera peridotite massif. *Journal of Petrology* **34**, 125–172.

Pertermann, M. & Hirschmann, M. M. (2003). Partial melting experiments on a MORB-like pyroxenite between 2 and 3 GPa: constraints on the presence of pyroxenite in basalt source regions from solidus location and melting rate. *Journal of Geophysical Research* **108**, paper number 2000JB000118.

Phipps Morgan, J. (1999). Isotope topology of individual hotspot basalt arrays: mixing curves or melt extraction trajectories. *Geochemistry, Geophysics, Geosystems* **1**, paper number 1999GC000004.

Phipps Morgan, J. (2001). Thermodynamics of pressure release melting of veined plum pudding mantle. *Geochemistry, Geophysics, Geosystems* **1**, paper number 1999GC000049.

Phipps Morgan, J. & Morgan, W. J. (1999). Two-stage melting and the geochemical evolution of the mantle: a recipe for mantle plum-pudding. *Earth and Planetary Science Letters* **170**, 215–239.

Phipps Morgan, J., Morgan, W. J., Zhang, Y.-S. & Smith, W. H. F. (1995). Observational hints for a plume-fed sub-oceanic asthenosphere and its role in mantle convection. *Journal of Geophysical Research* **100**, 12753–12768.

Robinson, J. A. C. & Wood, B. J. (1998). The depth to the spinel to garnet transition at the peridotite solidus. *Earth and Planetary Science Letters* **164**, 277–284.

Robinson, J. A. C., Wood, B. J. & Blundy, J. D. (1998). The beginning of melting of fertile and depleted peridotite at 1·5 GPa. *Earth and Planetary Science Letters* **155**, 97–117.

Salters, V. J. M. & Dick, H. J. B. (2002). Mineralogy of the mid-ocean ridge basalt source from neodymium isotopic composition of abyssal peridotites. *Nature* **418**, 68–72.

Salters, V. J. M. & Longhi, J. (1999). Trace element partitioning during the initial stages of melting beneath mid-ocean ridges. *Earth and Planetary Science Letters* **166**, 15–30.

Salters, V. J. M. & Stracke, A. (2004). Composition of the depleted mantle. *Geochemistry, Geophysics, Geosystems* **5**, paper number 2003GC000597.

Salters, V. J. M., Longhi, J. E. & Bizimis, M. (2002). Near mantle solidus trace element partitioning at pressures up to 3·4 GPa. *Geochemistry, Geophysics, Geosystems* **3**, paper number 2001GC000148.

Schilling, J.-G. (1969). Afar mantle plume: rare earth evidence. *Nature, Physical Science* **242**, 2–5.

Schilling, J.-G. (1973). The Icelandic mantle plume: geochemical study of the Reykjanes Ridge. *Nature* **242**, 565–571.

Schilling, J.-G., Kingsley, R. H., Hanan, B. B. & McCully, B. L. (1992). Nd–Sr–Pb isotopic variations along the Gulf of Aden: evidence for Afar mantle plume–continental lithosphere interaction. *Journal of Geophysical Research* **97**, 10927–10966.

Schwab, B. E. & Johnson, A. D. (2001). Melting systematics of modally variable, compositionally intermediate peridotites and the effects of mantle fertility. *Journal of Petrology* **42**, 1789–1811.

Shaw, D. M. (1970). Trace element fractionation during anatexis. *Geochimica et Cosmochimica Acta* **34**, 237–243.

Sleep, N. H. (1984). Tapping of magmas from ubiquitous mantle heterogeneities: an alternative to mantle plumes? *Journal of Geophysical Research* **89**, 10029–10041.

Snow, J. E., Hart, S. R. & Dick, H. J. B. (1994). Nd and Sr isotope evidence linking mid-ocean ridge basalts and abyssal peridotites. *Nature* **371**, 57–60.

Thirlwall, M. F., Gee, M. A. M., Taylor, R. N. & Murton, B. J. (2004). Mantle components in Iceland and adjacent ridges investigated using double-spike Pb isotope ratios. *Geochimica et Cosmochimica Acta* **68**, 361–386.

Van Westrenen, W., Blundy, J. D. & Wood, B. J. (2001). High field strength element/rare earth element fractionation during partial melting in the presence of garnet: implications for the identification of mantle heterogeneities. *Geochemistry, Geophysics, Geosystems* **2**, paper number 2000GC000133.

Walter, M. J. (1998). Melting of garnet peridotite and the origin of komatiite and depleted lithosphere. *Journal of Petrology* **79**, 29–60.

Walter, M. J. (1999). Comments on 'Mantle melting and melt extraction processes beneath ocean ridges: evidence from abyssal peridotites' by Yaoling Niu. *Journal of Petrology* **40**, 1187–1193.

Walter, M. & Presnall, D. C. (1994). Melting behaviour in simplified lherzolite in the system CaO–MgO–Al_2O_3–SiO_2–Na_2O from 7 to 35 kbar. *Journal of Petrology* **35**, 329–359.

Walter, M. J., Sisson, T. W. & Presnall, D. C. (1995). A mass proportion method for calculating melting reactions and application to melting of model upper mantle lherzolite. *Earth and Planetary Science Letters* **135**, 77–90.

Widom, E., Carlson, R. W., Gill, J. B. & Schmincke, H.-U. (1997). Th–Sr–Nd–Pb isotope and trace element evidence for the origin of the Sao Miguel, Azores, enriched mantle source. *Chemical Geology* **140**, 49–68.

Wood, B. J. & Blundy, J. D. (1997). A predictive model for rare earth partitioning between clinopyroxene and anhydrous silicate melt. *Contributions to Mineralogy and Petrology* **129**, 166–181.

Woodhead, J., Eggins, S. & Gamble, J. (1993). High field strength and transition element systematics in island arc and back-arc basin basalts: evidence for multi-phase melt extraction and a depleted mantle wedge. *Earth and Planetary Science Letters* **114**, 491–504.

Yasuda, A., Fujii, T. & Kurita, K. (1994). Melting phase relations of an anhydrous mid-ocean ridge basalt from 3 to 20 GPa: implications for the behaviour of subducted oceanic crust in the mantle. *Journal of Geophysical Research* **99**, 9401–9414.

Yaxley, G. M. (2000). Experimental study of the phase and melting relations of homogeneous basalt + peridotite mixtures and implications for the genesis of flood basalts. *Contributions to Mineralogy and Petrology* **139**, 326–338.

Yaxley, G. M. & Green, D. H. (1998). Reactions between eclogite and peridotite: mantle refertilisation by subduction of oceanic crust. *Schweitzerische Mineralogische und Petrographische Mitteilungen* **78**, 243–255.

Yu, D., Fontignie, D. & Schilling, J.-G. (1997). Mantle plume–ridge interactions in the Central North Atlantic: a Nd isotope study of Mid-Atlantic Ridge basalts from 30°N to 50°N. *Earth and Planetary Science Letters* **146**, 259–272.

Zindler, A., Staudigel, H. & Batiza, R. (1984). Isotope and trace element geochemistry of young Pacific seamounts: implications for the scale of upper mantle heterogeneity. *Earth and Planetary Science Letters* **70**, 175–195.

APPENDIX A: ADDITIONAL PRECONDITIONING AND MELTING EQUATIONS

Mantle preconditioning equations: calculation of trace element contents of residual matrix and residual plums

The trace element contents of the matrix and plum residues resulting from fractional melting [as used in equations (5) and (6) in the text] were given by Shaw (1970):

$$T^{M^*} = \left[\frac{T^{o}_{M}}{1 - rF_P}\right]\left[1 - \frac{P_M rF_P}{D^{o}_{M}}\right]^{1/P_M} \quad \text{(A1)}$$

$$T^{P^*} = \left[\frac{T^{o}_{P}}{1 - F_P}\right]\left[1 - \frac{P_P F_P}{D^{o}_{P}}\right]^{1/P_P} \quad \text{(A2)}$$

where D^{o} is the bulk distribution coefficient for a given element made up of partition coefficients (D_α) weighted according to the mass fractions of phases (X^{o}_α) at the start of melting $= \sum D_\alpha X^{o}_\alpha$ and with trapped melt treated as a phase with $D = 1$. P is the bulk reaction coefficient for a given element made up of partition coefficients (D_α) weighted according to the proportion of phases entering the melt (p_α) $= \sum D_\alpha p_\alpha$. Other symbols are defined in the text.

Equations for preconditioning with chemical exchange between plums and matrix

Equations (5) and (6) in the text may be modified to incorporate chemical exchange by including a trapped melt component of mass fraction F_T and with isotope and trace element concentrations I^L and T^L:

$$T^{A_R}_{2/1} = \frac{T^{P^*}_2 M_P(1 - zF_L) + T^{M^*}_2(1 - M_P)(1 - rzF_L) + F_T T^{L}_2(1 - F_L)}{T^{P^*}_1 M_P(1 - zF_L) + T^{M^*}_1(1 - M_P)(1 - rzF_L) + F_T T^{L}_1(1 - F_L)} \quad \text{(A3)}$$

$$I^{A_R}_1 = \frac{T^{P^*}_1 M_P(1 - zF_L) I^{P}_1 + T^{M^*}_1(1 - M_P)(1 - rzF_L) I^{M}_1 + T^{L}_1 F_T I^{L}_1(1 - F_L)}{T^{P^*}_1 M_P(1 - zF_L) + T^{M^*}_1(1 - M_P)(1 - rzF_L) + T^{L}_1 F_T(1 - F_L)} \quad \text{(A4)}$$

where, from Shaw (1970) and using symbols defined in Section 1.1 of his Appendix A, the trace element concentrations of the melt contributed by the matrix and plums are

$$T^{L}_M = \left(\frac{T^{o}_M}{F_M}\right)\left[1 - \left(1 - \frac{P_M F_M}{D^{o}_M}\right)^{1/P_M}\right]$$

$$T^{L}_P = \left(\frac{T^{o}_P}{F_P}\right)\left[1 - \left(1 - \frac{P_P F_P}{D^{o}_P}\right)^{1/P_P}\right]$$

and the overall trace element and isotope contents of the pooled melt are given by mass balance as

$$T^{L} = \frac{M_P z T^{L}_P + (1 - M_P) rz T^{L}_M}{M_P T^{L}_P + (1 - M_P) r T^{L}_M}$$

$$I^{L} = \frac{M_P T^{L}_P I^{L}_P + (1 - M_P) r T^{L}_M T^{L}_M}{M_P T^{L}_P + (1 - M_P) r T^{L}_M}.$$

Equations for dynamic melting of heterogeneous mantle

The melt derived from the plums and matrix can be converted to overall melt composition by application of the mixing equations

$$T^{L}_{2/1} = \frac{T^{L_P}_2 M_P F_P + T^{L_M}_2(1 - M_P) F_M}{T^{L_P}_1 M_P F_P + T^{L_M}_1(1 - M_P) F_M} \quad \text{(A5)}$$

$$I^{L}_1 = \frac{I^{P}_1 T^{L_P}_1 M_P F_P + I^{M}_1 T^{L_M}_1(1 - M_P) F_M}{T^{L_P}_1 M_P F_P + T^{L_M}_1(1 - M_P) F_M} \quad \text{(A6)}$$

where the superscript L refers to the bulk melt, L_P to the melt contributed by the 'plum' end-member and L_M to ratios the melt contributed by the matrix end-member. As with melt extraction, the trace element concentrations (T_1) they contain can be modelled using the fractional melting equation for pooled fractional melting of Appendix A, Section 1.2 of Shaw (1970).

Given that, as before, $F_M = rF_P$, the equations become

$$T^{L}_{2/1} = \frac{T^{L_P}_2 M_P + r T^{L_M}_2(1 - M_P)}{T^{L_P}_1 M_P + r T^{L_M}_1(1 - M_P)} \quad \text{(A7)}$$

$$I_1^{\mathrm{L}} = \frac{I_1^{\mathrm{P}} T_1^{\mathrm{L_P}} M_{\mathrm{P}} + r I_1^{\mathrm{M}} T_1^{\mathrm{L_M}} (1 - M_{\mathrm{P}})}{T_1^{\mathrm{L_P}} M_{\mathrm{P}} + r T_1^{\mathrm{L_M}} (1 - M_{\mathrm{P}})}. \quad \text{(A8)}$$

APPENDIX B: ESTIMATING MINERAL PROPORTIONS FROM CaO AND Al_2O_3 CONCENTRATIONS

(1) The equations can be obtained by rearranging simultaneous mass balance equations. For three minerals with mass fractions X_α, X_β and X_γ containing CaO concentrations of CaO_α, CaO_β and CaO_γ and Al_2O_3 concentrations of $Al_2O_{3\alpha}$, $Al_2O_{3\beta}$ and $Al_2O_{3\gamma}$ making up bulk-rock concentrations of CaO_{tot}, Al_2O_{3tot}

$$CaO_{tot} = X_\alpha CaO_\alpha + X_\beta CaO_\beta + X_\gamma CaO_\gamma$$

$$Al_2O_{3tot} = X_\alpha Al_2O_{3\alpha} + X_\beta Al_2O_{3\beta} + X_\gamma Al_2O_{3\gamma}.$$

Because $X_\gamma = 1 - X_\alpha + X_\beta$, the equations can be solved for X_α and X_β:

$$X_\alpha = \frac{(ab - cd)}{(eb - fd)} \quad \text{(B1)}$$

$$X_\beta = \frac{(af - ce)}{(df - be)} \quad \text{(B2)}$$

where

$$\begin{aligned} a &= Al_2O_{3tot} - Al_2O_{3\gamma} \\ b &= CaO_\beta - CaO_\gamma \\ c &= CaO_{tot} - CaO_\gamma \\ d &= Al_2O_{3\beta} - Al_2O_{3\gamma} \\ e &= Al_2O_{3\alpha} - Al_2O_{3o\gamma} \\ f &= CaO_\alpha - CaO_\gamma \\ X_\gamma &= 1 - (X_\alpha + X_\beta). \end{aligned} \quad \text{(B3)}$$

(2) If a fourth mineral with mass fraction X_δ is added, its mass fraction must be estimated independently. In addition, the total concentrations of Al_2O_3 and CaO must then be recalculated by subtracting the contribution of the fourth phase:

$$\begin{aligned} Al_2O_3^* &= \frac{Al_2O_{3tot} - X_\delta Al_2O_{3\delta}}{1 - X_\delta} \\ CaO^* &= \frac{CaO_{tot} - X_\delta CaO_\delta}{1 - X_\delta}. \end{aligned} \quad \text{(B4)}$$

$$X_\alpha = (1 - X_\delta)\frac{(Ab - Cd)}{(eb - fd)} \quad \text{(B5)}$$

$$X_\beta = (1 - X_\delta)\frac{(Af - Ce)}{(df - be)} \quad \text{(B6)}$$

where $A = Al_2O_3^* - Al_2O_{3\gamma}$ and $C = CaO^* - CaO_\gamma$. Then

$$X_\gamma = 1 - (X_\alpha + X_\beta + X_\delta). \quad \text{(B7)}$$

(3) If $P > 3{\cdot}3$ GPa, the calculation can be performed with α for clinopyroxene, β for garnet, and γ for olivine using equations (B1)–(B3).

(4) If $P = 3{\cdot}3$–$2{\cdot}8$ GPa, the calculation can be performed with α for clinopyroxene, β for orthopyroxene, γ for olivine and δ for garnet using equations (B4)–(B7).

$X_\delta = X_{gt}$ must first be estimated at the chosen pressure, P, assuming a linear decrease in the mass fraction of garnet from 3·3 to 2·8 GPa:

$$X_{gt} = X_{gt}^{3{\cdot}5\mathrm{GPa}} \frac{P - 2{\cdot}8}{3{\cdot}5 - 2{\cdot}8}. \quad \text{(B8)}$$

(5) If $P < 2{\cdot}8$ GPa, the calculation can be performed with α for clinopyroxene, β for orthopyroxene, γ for olivine and δ for spinel using equations (B4)–(B7).

$X_\delta = X_{sp}$ must first be estimated at the chosen pressure, P, assuming a linear decrease in the mass fraction of spinel from 2·8 to 1·0 GPa, determined by mass balance, resulting from the decrease in aluminium content of pyroxenes:

$$X_{sp} = 0{\cdot}039 - 0{\cdot}01P. \quad \text{(B9)}$$

APPENDIX C: RECALCULATION OF MINERAL PROPORTIONS AFTER EACH EXTRACTION EPISODE

After a melt extraction episode and loss of a melt fraction, F_L, the mass fractions of plums and matrix are given by

$$\begin{aligned} M_{\mathrm{P}} &= \frac{F_{\mathrm{P}} M_{\mathrm{P}}^*}{1 - F_{\mathrm{L}}} \\ M_{\mathrm{M}} &= 1 - M_{\mathrm{P}}. \end{aligned}$$

The Yb, Nd and Nd isotope composition of plums and matrix can then be calculated using reset values of M_p and M_M and assuming incorporation of the trapped melt:

$$T_{\mathrm{M}} = \frac{M_{\mathrm{M}} T_{\mathrm{M}}^* + F_{\mathrm{T}} T^{\mathrm{L}}}{M_{\mathrm{M}} + F_{\mathrm{T}}} \quad \text{(C1)}$$

$$T_{\mathrm{P}} = \frac{M_{\mathrm{P}} T_{\mathrm{P}}^* + F_{\mathrm{T}} T^{\mathrm{L}}}{M_{\mathrm{P}} + F_{\mathrm{T}}} \quad \text{(C2)}$$

$$I_{\mathrm{M}} = \frac{M_{\mathrm{M}} T_{\mathrm{M}} I_{\mathrm{M}}^{\mathrm{L}} + F_{\mathrm{T}} T^{\mathrm{L}} I^{\mathrm{L}}}{M_{\mathrm{M}} T_{\mathrm{M}} + F_{\mathrm{T}} T^{\mathrm{L}}} \tag{C3}$$

$$I_{\mathrm{P}} = \frac{M_{\mathrm{P}} T_{\mathrm{P}} I_{\mathrm{P}}^{\mathrm{L}} + F_{\mathrm{T}} T^{\mathrm{L}} I^{\mathrm{L}}}{M_{\mathrm{P}} T_{\mathrm{P}} + F_{\mathrm{T}} T^{\mathrm{L}}} \tag{C4}$$

The source mineralogy at the pressure of melt extraction can then be calculated. For each phase (α) and for each oxide, the concentrations, X_{M} and X_{P}, in the matrix and plum residues may be estimated using the reaction coefficient (p_α) as

$$X_{\mathrm{M}}^{*} = \frac{X_{\mathrm{M}} - p_\alpha F_{\mathrm{M}}}{(1 - F_{\mathrm{M}})} \tag{C5}$$

$$X_{\mathrm{P}}^{*} = \frac{X_{\mathrm{P}} - p_\alpha F_{\mathrm{P}}}{(1 - F_{\mathrm{P}})}. \tag{C6}$$

The CaO and Al_2O_3 contents of the matrix and plums can then be calculated in preparation for determining the source mineralogy for future extraction events. The matrix and plums are calculated separately so that, for each oxide, the concentration in the residue is given by

$$\begin{aligned} \mathrm{CaO} &= \sum \mathrm{CaO}_\alpha^{*} X_\alpha^{*} \\ \mathrm{Al_2O_3} &= \sum \mathrm{Al_2O_{3\alpha}^{*}} X_\alpha^{*}. \end{aligned} \tag{C7}$$